Influence of redox processes on the germanium isotopic composition of ordinary chondrites

Guillaume Florin, Béatrice Luais, Tracy Rushmer, Olivier Alard

Journal Pre-proofs

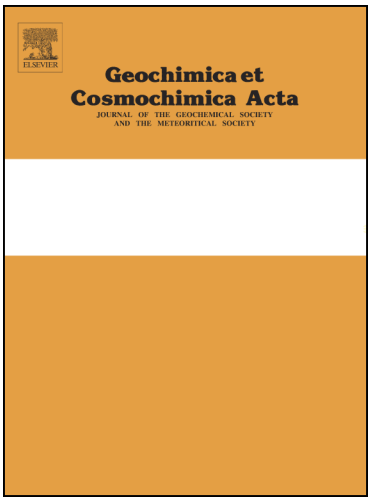

Influence of redox processes on the germanium isotopic composition of ordinary chondrites

Guillaume Florin, Béatrice Luais, Tracy Rushmer, Olivier Alard

PII: S0016-7037(19)30692-1
DOI: https://doi.org/10.1016/j.gca.2019.10.038
Reference: GCA 11506

To appear in: *Geochimica et Cosmochimica Acta*

Received Date: 29 May 2019
Accepted Date: 28 October 2019

Please cite this article as: Florin, G., Luais, B., Rushmer, T., Alard, O., Influence of redox processes on the germanium isotopic composition of ordinary chondrites, *Geochimica et Cosmochimica Acta* (2019), doi: https://doi.org/10.1016/j.gca.2019.10.038

Influence of redox processes on the germanium isotopic composition of ordinary chondrites

Guillaume Florin[a,*], Béatrice Luais[a], Tracy Rushmer[b], Olivier Alard[b,c]

[a]: Centre de Recherches Pétrographiques et Géochimiques, CRPG-CNRS- UMR 7358, Université de Lorraine, 15 Rue Notre Dame des Pauvres, 54500 Vandœuvre-lès-Nancy, France

[b]: Department of Earth and Planetary Sciences, Macquarie University, NSW 2109, Australia

[c]: Géosciences Montpellier, UMR 5243, CNRS & Université Montpellier, 34095 Montpellier, France.

*: Corresponding author guillaume.florin@univ-lorraine.fr

Abstract

Ordinary chondrites (OCs) are classified into three groups, according to their oxidation state, which increases from the H to L to LL groups. This is demonstrated by the decrease in metal content (H=~8 vol%, L=~4 vol%, and LL=~2 vol%), and by a positive correlation between $\Delta^{17}O$ and %Fa through the OC sequence. Compared to other chondrites, OCs exhibit the largest variation in oxidation state but there is an ongoing debate on the processes that control this variation. To constrain the causes of the variations in the oxidation state with respect to the associated nebular versus parent bodies processes, we investigated the elemental and isotopic

variations of germanium (moderately siderophile and volatile) in the bulk sample, as well as in the metal, silicate and sulfide phases, over a range of petrographic types for the H, L, and LL ordinary chondrites.

We found that $\delta^{74/70}Ge_{metal}$ is a proxy for the $\delta^{74/70}Ge_{bulk}$ composition and that each OC group is distinguishable by their $\delta^{74/70}Ge_{metal}$, which increases from –0.51±0.09‰ for H chondrites, –0.31±0.06‰ for L chondrites, and, finally, to –0.26±0.09‰ for LL chondrites (2σSD). Additionally, the OC sequence exhibited a positive correlation, from H to L to LL, between $\delta^{74/70}Ge_{metal}$ and %Fa, as well as oxygen isotopes ($\delta^{17}O$, $\delta^{18}O$ and $\Delta^{17}O$), that was not a consequence of a "size sorting effect" on chondrules (*i.e.* chondrule mixing) or metamorphic processes in the parent bodies but, rather, was the result of nebular processes. We propose that the correlation between the $\delta^{74/70}Ge$ values and %Fa, $\Delta^{17}O$, $\delta^{18}O$ can be explained by an increasing proportion of accreted hydrated phyllosilicates, from the H, L to LL groups, with high $\delta^{74/70}Ge$ and $\Delta^{17}O$. We found that 10 to 15% of phyllosilicates, with a composition of [Ge]=4–7 ppm and $\delta^{74/70}Ge$=3–2.5‰, is needed to change the $\delta^{74/70}Ge$ from H to LL, which corresponds to a $\Delta^{17}O$≈8-7‰. This value agrees with the $\Delta^{17}O$≈7‰ composition of the accreted nebular component reported by Choi et al. (1998). During thermal metamorphism, phyllosilicates destabilize, liberating germanium that will be incorporated in the metal, then leading to its high $\delta^{74/70}Ge$ signature.

High-temperature metamorphism can explain the lack of $\delta^{74/70}Ge_{metal}$ variation with the petrologic type in the OC, even for the type 3 chondrites (T≈675°C), implying a complete reaction even at low petrologic types. In addition, metal-silicate re-equilibration in response to thermal metamorphism results in a decrease in $\Delta^{74/70}Ge_{metal\text{-}silicate}$ from 0.33‰ to 0.06‰, within the H chondrite group, which is interpreted as the result of $\delta^{74/70}Ge_{silicate}$ variation. The mean positive $\Delta^{74/70}Ge_{metal\text{-}silicate}$ fractionation factor of +0.22±0.36‰ (error propagation on individual error) also displays a remarkable similarity to the direction of isotopic fractionation with other germanium

isotopic metal-silicate datasets, such as the magmatic iron meteorites, the Earth silicate reservoirs. We propose that the $\Delta^{74/70}Ge_{metal\text{-}silicate}$ and the negative $\delta^{74/70}Ge$ values of OCs are inherited from metal-silicate melting and partial exchange before planetesimal accretion in a light isotope-enriched gas. Finally, the $\delta^{74/70}Ge_{metal}$-$\Delta^{17}O_{silicate}$ correlation between the IIE iron meteorites and OCs, provides new evidence for the existence of a highly reduced HH group.

1. Introduction

Ordinary chondrites (OCs) are undifferentiated meteorites that formed in the first 1 to 3 Myr after the formation of refractory Calcium-Aluminium Inclusions (CAIs) (Kleine *et al.*, 2008; Archer *et al.*, 2019; Hellmann *et al.*, 2019), as well as during a short accretion time interval of less than 0.5 Myr (Monnereau *et al.*, 2013). OCs also postdate magmatic iron meteorite formation. Several studies argue for their formation via the disruption-re-accretion of early-differentiated planetesimals (Elkins-Tanton *et al.*, 2011; Lichtenberg *et al.*, 2018). As a result, OCs should represent a record between the early formed planetesimals and terrestrial planets as we know them today.

Ordinary chondrites are composed of an assemblage of chondrules and matrix, which contain silicates, FeNi alloys, sulfides, and rare CAIs. The OC sequence has been classified into three groups, *i.e.*, H (High metallic Fe content), L (low metallic Fe content) and LL (low total Fe and low metallic Fe content), according to the oxidized iron content relative to the metal iron (Urey and Craig, 1953), oxygen isotopic composition (Clayton *et al.*, 1991), bulk volatile elemental concentration, including water, and chondrule size (Wasson, 1972; Chou and Cohen, 1973; Chou *et al.*, 1973; Kallemeyn *et al.*, 1989; Wasson, 2000; Rubin, 2005). Each chondrite group is thought to originate from at least one parent body and are subdivided into petrologic types, from the least metamorphosed and unequilibrated (group 3) to the most metamorphosed

and highly equilibrated (group 6; Van Schmus and Wood, 1967). Studies on OC ages, cooling times, and petrographic types led to the creation of the "onion-shell" model in which thermal metamorphism increases with planetesimal depth (Göpel *et al.*, 1994). With increasing petrographic type, the temperature (Tait *et al.*, 2014) and oxidation state increase (Chou and Cohen, 1973; Chou *et al.*, 1973; Rubin, 2005), metallic iron content decreases, and metal becomes more equilibrated with silicate through oxidation reactions (McSween and Labotka, 1993). Moreover, as thermal metamorphism increases, the metal grain-size, as well as the grain circularity, increase, which define additional parameters for characterizing the petrologic types (Guignard and Toplis, 2015).

The percentage of fayalite in olivine (%Fa) is commonly used as a redox proxy (Chou *et al.*, 1973; Rubin, 2005). Clayton *et al.* (1991) first showed that there was an increase in the oxygen isotopic composition from the H to LL groups, which led McSween and Labotka (1993) and Rubin (2005) to demonstrate that there is a positive correlation between %Fa and the oxygen isotopic composition throughout the OC sequence. This implies that variations in $\delta^{18}O$ and $\Delta^{17}O$ are related to the oxidation state. However, the origin of oxidation processes remains highly controversial. Previous studies have argued that this evolution reflects primitive conditions in the solar nebula recorded by planetesimals through progressive accretion of high $\Delta^{17}O$ nebula water hosted in phyllosilicates (*i.e.* Rubin, 2005). Thermal metamorphism, induced by heat release from the decay of short-lived radioactive elements (^{26}Al), liberates heavy-O water, which produces both an increase in the oxidation state and oxygen isotopic composition. On the other hand, the oxidation state can also be explained by an increase in the proportion of type II chondrules (oxidized) and the decrease of type I chondrules (reduced) from H to LL. Type I is reduced, O^{16}-rich, and contain metallic Fe, whereas type II is oxidized, ^{16}O-depleted, and Fe is present in an oxidized form (Zanda *et al.*, 2006). Chou and Cohen (1973) and Chou *et al.* (1973) have shown that OCs groups are also resolvable using the siderophile element concentration,

e.g., the germanium content in the metal increases from H to LL with the Ni content, as a proxy of the redox state. They proposed that a significant proportion of Ge condenses in the silicate at its formation, such that Ge is redistributed between the metal and silicate through oxidation-reduction during metamorphic processes on their parent bodies.

Germanium is a moderately siderophile and volatile element ($T_{50\%\ condensation}$ = 883K at $pH_2O/pH_2 = 4.2 * 10^{-4}$ atm; Lodders *et al.*, 2009), commonly used with Ir, Au, and Ni to constrain the formation of iron meteorites and metal phases in chondrites (Wasson, 1974). Experimental studies have shown that Ge partitioning between metal and silicate phases is strongly redox-dependent, with D(Ge) metal-silicate values greater than 10^4 under highly reduced conditions (–2.7 log fO_2 relative to the IW buffer; Kegler and Holzheid, 2011). Germanium is also a chalcophile element but the amount of Ge in troilite (FeS) from the OCs represents only 3 to 5% (0.3 to 0.5 ppm) of the total amount of Ge in OCs (Chou and Cohen, 1973; Wai and Wasson, 1979), whereas it is strongly concentrated, *i.e.*, up to several hundred ppm, in terrestrial low-temperature sulfides (Bernstein, 1985).

Germanium has five stable isotopes, *i.e.*, ^{70}Ge, ^{72}Ge, ^{73}Ge, ^{74}Ge, and ^{76}Ge, with the Ge isotopic composition given as a delta notation: $\delta^{74/70}Ge = (((^{74}Ge/^{70}Ge_{Sample} / {}^{74}Ge/^{70}Ge_{Standard}) - 1) \times 1000$. To date, previous studies have analyzed the germanium isotopic composition of differentiated bodies that experienced metal-silicate segregation to investigate the conditions and processes of planetary differentiation. Magmatic iron meteorites that represent planetesimal cores display positive and heavier Ge isotopic compositions than the Earth's mantle and crust (Luais, 2007; Luais, 2012). The Ge isotopic composition of the Earth's silicate reservoir is, thus far, homogeneous and has not been significantly modified by complex crust–mantle exchange via fluids in subduction zones (El Korh *et al.*, 2017).The volatile behavior of germanium can also be responsible for large Ge isotopic fractionations that occur in IIE non-magmatic iron meteorites (Luais, 2007), which form due to metal segregation following impact-driven melting at the sub-

surface of their parental bodies (Wasson and Wang, 1986; Wasson, 2017). To date, the only constituents that display strong negative $\delta^{74/70}$Ge values are schreibersite (Fe-Ni-P) inclusions in iron meteorites (Rouxel and Luais, 2017) and low-temperature terrestrial Zn-sulfides (Belissont *et al.*, 2014). Metal-silicate segregation, volatility, and phosphide/sulfide exsolution/crystallization are the main processes, currently known, that strongly fractionate germanium and its isotopes.

Germanium isotopes represent potential tools to investigate processes of formation and evolution of ordinary chondrites (1) during condensation of metal-silicate-sulfide from the solar nebula (Sears, 1978; Wai and Wasson, 1979), (2) by inheritance from previously destroyed planetesimals (Litchenberg *et al.*, 2018), and (3) metal-silicate equilibrium fractionation on parent bodies following a major impact (Tomkins *et al.*, 2013) or after metamorphism (Humayun and Campbell, 2002; Guignard and Toplis, 2015). In addition, ordinary chondrites provide a suitable environment to explore the relationships between Ge and O isotopes, as well as the redox conditions. The combined use of these data can establish constraints on the environment in which OCs form and the processes that lead to metal-silicate fractionation and equilibration. Germanium isotopic measurements on separated phases from unequilibrated and equilibrated OCs are used to evaluate the effect that metamorphism has on metal-silicate isotope fractionation. Clayton *et al.* (1991) first proposed the genetic association between ordinary chondrites and IIE iron meteorites based on their oxygen isotopic compositions in silicate clasts. The IIE–OCs relationship has been further constrained with Mo isotopic anomalies (Burkhardt *et al.*, 2011; Budde *et al.*, 2016). Here, based on the Ge isotopic composition in the metal phase, we examine a new genetic link between IIE iron meteorites and H OCs.

2. Samples and methods

2.1. Sample selection

To constrain the metamorphic and shock effects on Ge systematics, sixteen OCs (eight H, six L, and two LL) were selected to represent all petrologic types (Van Schumus and Wood, 1967) and various shock stages as defined by (Stöffler *et al.*, 1991). In addition, two samples were specifically selected to assess the effect of shock: Rose City, an impact melt breccia, and Portales Valley, a low shock meteorite with large metal veins as an example of metal migration (Ruzicka *et al.*, 2005). Table 1 summarizes the sample characteristics.

2.2. Analytical Procedures

2.2.1. Sample preparation

Approximately 500 mg of initial bulk meteorite material was cleaned with 0.2 M HNO_3 under cold ultrasonic agitation for 5 minutes. The acid was removed, the samples were rinsed with pure water under ultrasonic agitation and then rinsed with acetone to avoid metal oxidation. Afterward, 300 mg of the meteorite sample was gently powdered in an agate mortar for bulk elemental and isotopic measurements.

Metal and sulfide separation. The remaining 200 mg of clean sample was gently crushed in an agate mortar. FeNi metal was removed from the crushed sample with a hand-magnet. The magnetic fraction was crushed multiple times in an agate mortar, followed by several minutes of ultrasonic agitation in an acetone medium to remove all silicate particles remaining on the metal surface. A Frantz magnetic separator was used to separate the sulfides from the remaining weakly magnetic powder. Between 10 and 40 mg of metal and 10 to 20 mg of sulfide were separated using these procedures.

Silicate separation. The crushed non-magnetic sample fraction that mostly contained impure silicates was gently grounded in an agate mortar to a fine powder. To remove the non-magnetic sulfides and small metal particles stuck on the silicates, two successive cleanings with 6 M HCl

and 2 M HNO_3 were performed for 5 minutes under ultrasonic agitation at room temperature. As Ge is highly volatile when associated with HCl at a high temperature (T > 60°C), this protocol was first tested on San Carlos olivine samples to evaluate Ge loss. Uncleaned olivines have [Ge] = 0.89 ± 0.02 ppm and $\delta^{74/70}$Ge = 0.70 ± 0.08‰ while clean olivines have [Ge] = 0.90 ± 0.02 ppm and $\delta^{74/70}$Ge = 0.71 ± 0.09‰ (Table 2), which demonstrates that there was no Ge loss nor isotopic fractionation during cold HCl leaching. This step is important because metallic phases are at least one hundred times more concentrated in germanium than silicates or sulfides (Chou and Cohen, 1973). The presence of small metal particles on the silicate surface would have introduced a bias on the elemental and isotopic compositions of Ge in silicates.

Chondrule separation. Separation was only performed on Dhajala (H3.8). A total of 1 g of Dhajala was cleaned and gently crushed in an agate mortar to preserve the chondrules. Unbroken chondrules were separated by hand-picking and sieved into two fractions, *i.e.*, 100–300 µm and > 300 µm, with a recovery of 9.1 and 130.5 mg, respectively.

All fractions were later checked and purified by hand-picking under a binocular microscope, successively cleaned with diluted HNO_3, distilled H_2O, and acetone under cold ultrasonic agitation, and dried under a laminar flow hood.

2.2.2. Sample digestion and chemical purification of germanium

The germanium chemistry analytical procedures for metal, sulfide, and silicate phases follow those described in Luais (2007, 2012, references therein) and Belissont *et al.* (2014). Samples were dissolved in Teflon beakers on a hotplate in concentrated HF-HNO_3 solutions for the silicate and sulfide fractions while metal phases were dissolved in an HNO_3-only solution. Bulk samples were digested under pressure (25 bar) using Bola Teflon bombs at 150°C (Luais *et al.*, 2009) for one week in an oven to ensure the dissolution of all phases, including chromite. To

ensure that no Ge was lost at high temperatures under pressure, this protocol was tested using a BIR-1 geo-standard. We obtained a $\delta^{74/70}$Ge of 0.59 ± 0.10‰ for BIR-1 that was digested in the bomb while this was $\delta^{74/70}$Ge = 0.59 ± 0.06‰ for conventional hotplate BIR-1 dissolution. This demonstrates that there was no isotopic fractionation using this digestion method (Table 2). Germanium purification from silicate and sulfide matrices was completed in two steps using ion exchange resins. First, anionic resin (AG1-X8 resin chloride form, 200 – 400 mesh, Biorad, Hercules, CA, U.S.A.) allowed us to eliminate most elements (*i.e.*, the alkalis, Mn, Al, Co, Ni, Zn, Ga, and most Fe) using 1 M HF. Germanium (± Fe, Mg) was eluted with 0.2 M HNO_3. Germanium purification from Fe and the remaining matrix was performed solely using cation exchange resin (AG 50W-X8, Biorad, 159 Hercules, CA, U.S.A.) and 0.5 M HNO_3. Germanium isolation from the Fe-Ni matrix of the metal phase was performed only using the cation exchange resin step. These two procedures had a germanium yield of 100% within error (Luais, 2007; Luais, 2012). All acids used for digestion and germanium chemical separation were high-purity grade SeaStar® reagents.

2.2.3. Elemental measurements

Bulk powder samples and metal phase separates from H OCs, and metal from L samples were analyzed for major and trace elemental compositions including Ge at the SARM analytical facility (Service Analytique des Roches et des Minéraux, CRPG-Nancy) using a *ThermoFischer* ICP-MS *X7*. Errors associated with the Ge, Ni and Co measurement were < 5% for our sample concentrations. The separated mass of pure sulfides was low (*i.e.*, approximately 10 – 20 mg) due to their low occurrence in the OCs (~5.7%; Lauretta *et al.*, 1997). Similarly, only 10 – 40 mg of pure silicate separates were obtained. These available low mass fractions rule out the possibility of analyzing them using routine procedures at the SARM. These fractions were

analyzed for their Ge elemental compositions using a *ThermoFischer* ICP-MS *X-Series* at CRPG (Nancy, France) with a 2σ SD of 1.2%.

2.2.4 Ge isotopic measurements

Samples in a 0.5 M HNO_3 solution from the cation exchange step were analyzed for their Ge isotopic compositions using a Neptune*Plus* multiple-collector inductively coupled plasma mass spectrometer (MC-ICP-MS) at CRPG coupled with a hydride generator introduction system (HGIS). The HGIS method involves mixing the sample with a high-reducing solution of $NaBH_4$-NaOH. The reactions between these two solutions convert volatile aqueous species ($GeOH_4$) to gaseous ($GeH_{4\ (gas)}$) hydride species (Dedina and Tsalev, 1995; Abdul-Majeed and Zimmerman, 2012). As the reducing solution is in excess, the reaction yield is 100%. This technique removes isobaric interferences from elements that do not form hydrides, avoiding Zn, NiO, and FeO interferences, as well as matrix effects. The result is a gain in signal sensitivity of at least a factor of 30, required for routine isotopic measurements of 10 – 20 ng Ge (exceptionally down to 5 ng) to obtain high precision and a good external reproducibility of less than 0.1‰ (2σ SD) (see Rouxel and Luais, 2017 for more details). Data were acquired in static mode using the ^{68}Zn, ^{69}Ga, ^{70}Ge, ^{71}Ga, ^{72}Ge, ^{73}Ge, and ^{74}Ge isotopes that corresponded to the L3, L2, L1, C, H1, H2, and H3 Faraday cups, respectively. We report an intensity of 1.5 – 2.5 V on ^{74}Ge for a 10 ppb Ge standard solution. Each measurement was composed of a 320 s data acquisition sequence distributed over 40 cycles. Procedural Ge blanks, including chemistry and MC-ICPMS, were better than 70 pg and negligible as this represents less than 0.1% of the 100 ng of Ge processed for each sample. Sample measurements were bracketed using the NIST3120a Ge standard solution. Results are reported in delta (δ) notation using $^{x}Ge/^{70}Ge$ ratios with respect to the mean ratios of the NIST 3120a standard analyzed just before and after the sample (Luais, 2012):

$$\delta^{x/70}Ge_{NIST3120a} = \delta\ {}^{x}Ge/{}^{70}Ge = \left(\frac{({}^{x}Ge/{}^{70}Ge)_{Sample}}{({}^{x}Ge/{}^{70}Ge)_{NIST3120a}} - 1\right) * 1000. \qquad (1)$$

JMC and Aldrich germanium standard solutions were analyzed during the course of the study, yielding $\delta^{74/70}$Ge = –0.32 ± 0.11‰ (n = 95) and $\delta^{74/70}$Ge = –1.97 ± 0.12‰ (n = 99) (2σ SD), respectively. The BIR-1 basalt geostandard yielded $\delta^{74/70}$Ge = 0.63 ± 0.17‰ (n = 10) and the in-house IAB Magura iron meteorite (Luais, 2007) had a $\delta^{74/70}$Ge value of 0.78 ±0.08‰ (n = 19). These values agree with the references given in Luais (2012) and (Escoube *et al.*, 2012).

3. Results

3.1. Elemental composition

The majority of the bulk H OCs displayed a rather uniform Ge concentration, ranging from 10.3 to 22.2 ppm (mean = 15.8 ± 0.8 ppm; see Table 3 and Fig. 1) with no variation among the petrologic types, which is in agreement with $[Ge]_{mean}$ = 12.7 ± 1.5 ppm reported in Fouché and Smales, (1967) and similar to the value reported for L OCs in Tandon and Wasson (1968). However, Allegan H5 ([Ge] = 22.2 ppm, [Ni] = 1.52 wt. %) and Guareña ([Ge] = 21.4 ppm, [Ni] = 1.59 wt. %) had slightly higher Ge and Ni contents (see Fig. A2 in the Appendix) compared to the OC mean ([Ge] = 15.8 ± 0.8, $[Ni]_{mean}$ = 1.28 ± 0.54 wt. %) and bulk data reported by (Wasson and Kallemeyn, 1988). For these samples, this may be due to a sampling bias from either a high taenite zone or, although the main mass may appear to be homogeneous, a small-scale heterogeneous repartition of metal that led to the sampling of a metal-rich zone.

Germanium concentrations in metal ranged from 50 to 83.5 ppm for H chondrites, with a mean of 64.6 ± 17.6 ppm (2σ SD), 104.3 to 157.8 ppm for L chondrites, with a mean of 135.9 ± 53.2 ppm (2σ SD), and 85 to 120 ppm for LL chondrites, with a mean of 102.5 ± 49.5 ppm. These values are within those reported by Chou *et al.* (1973) and Chou and Cohen (1973), who

proposed that a significant amount of Ge in the silicates was redistributed in the metal during metamorphism. Moreover, the increase in the oxidation state from H to L to LL should have decreased the amount of the metal phase, and, consequently, increased the concentration of Ge in the metal. Taken together, all the metal samples define a positive correlation among Ge, Ni, and Co, demonstrating that taenite (Ni-rich) is more concentrated in Ge than kamacite (Ni-poor) (see Figure A in the Appendix).

Germanium concentrations in silicates from the H group ranged from 0.2 (H4 Ste Marguerite) to 2.2 ppm (H3.4 Sharps) (see Table 3 and Fig. 1), identical to the order of magnitude for data reported in Chou *et al.* (1973). However, we observed a discrepancy for the Allegan Ge concentration between our data, *i.e.*, 0.35 ppm compared with a value of 0.06 ppm reported in Chou *et al.* (1973). In the L group, Ge concentrations in silicates ranged from 0.05 ppm (L6 Alfianello) to 0.65 ppm (L4 Björbole) (Table 3 and Fig. 1). They are identical to the values reported by Chou and Cohen (1973)

The sulfides from H6 Kernouvé and H4 Ste Marguerite were strongly depleted in Ge, with concentrations of 1.75 and 1.95 ppb (see Table 3 and Fig. 1), respectively. This indicates the strong compatibility of Ge in the Fe-Ni metallic phase.

3.2. Germanium isotopic data

Germanium isotope measurements were performed on bulk samples, silicates, and sulfides from H group chondrites, whereas we only analyzed L samples for metal and silicate, and LL for metal (Table 3). All samples plot on the mass-dependent fractionation line (see Fig. B in the Appendix).

Bulk Ge isotopic compositions define a narrow range from $\delta^{74/70}$Ge = –0.59 ± 0.04‰ to –0.37 ± 0.15‰, with a mean of $\delta^{74/70}$Ge = –0.54 ± 0.09‰. Only Dhajala (with the highest $\delta^{74/70}$Ge

value at –0.37‰) deviated by more than 0.1‰ from the mean. Therefore, this sample ,was not included in the mean (see section 4.5 for explanation) (Fig. 2A).

The $\delta^{74/70}$Ge composition for metal from H group samples ranged from –0.33 ± 0.12‰ (Dhajala) to –0.57 ± 0.12‰ (metallic globules from Portales Valley), with a mean of –0.51 ± 0.09‰ (*N.B.* we excluded the Dhajala value due to its unusual Ge isotopic composition, see section 4.5 for explanation). The $\delta^{74/70}Ge_{metal}$ compositions for L group samples showed small variations from –0.35 ± 0.09‰ (Hedjaz) to –0.28 ± 0.01‰ (Alfianello), with a mean of $\delta^{74/70}$Ge = –0.31 ± 0.06‰. The LL group yielded a mean value of $\delta^{74/70}$Ge = –0.26 ± 0.09‰.

Silicates displayed lighter Ge isotopic compositions than bulk samples, with a large range in $\delta^{74/70}$Ge from –0.92‰ for Allegan (H5) to –0.50 ± 0.11‰ for Dhajala (H3), with a mean of –0.67 ± 0.33‰ for the H groups (Fig. 2A) and from -1.25 (Alfianello, L6) to -0.50 ± 0.09 (Bjürbole, L4) with a mean of –0.87 ± 0.18 for the L group (Fig. 3A).

The sulfides were analyzed in two samples, without replicates due to their low abundance in OCs and Ge concentration (≈ 2 ppb). They were characterized by the lightest isotopic values at $\delta^{74/70}$Ge = –1.60‰ (Ste Marguerite, H4) and $\delta^{74/70}$Ge = –1.56‰ (Kernouvé, H6). We attributed the highest error to these samples based on the standards at ± 0.20‰ (2σ SD) (Fig. 3).

The two chondrule fractions from Dhajala had similar isotopic compositions of $\delta^{74/70}$Ge = –0.28 ± 0.12‰ for < 300 µm chondrules and $\delta^{74/70}$Ge = –0.38 ± 0.11‰ for > 300 µm chondrules (Table 3).

3.3. Metal phases: main contributors to Ge isotopic compositions in bulk OCs

The metal phase is at least 60 times more concentrated in Ge than the silicates (Chou *et al.*, 1973) and four orders of magnitudes higher than sulfide (Fig. 3A). The germanium isotope

compositions of bulk H chondrites (mean $\delta^{74/70}Ge_{bulk}$ = –0.54 ± 0.09‰) were within error of the metal (mean $\delta^{74/70}Ge_{metal}$ = –0.51 ± 0.09‰), except for Sharps, and higher than the silicate (mean $\delta^{74/70}Ge_{silicate}$ = –0.67 ± 0.33‰). In a $\delta^{74/70}$Ge versus Log(1/Ge) diagram (Fig. 3B), the mixing line defined by the bulk sample, metal, silicate, and sulfide phases (mean $\delta^{74/70}Ge_{sulfide}$ = –1.56 ± 0.02‰), at all metamorphic grades, indicates that the $\delta^{74/70}$Ge measurements of separate phases are consistent with the $\delta^{74/70}$Ge measurements of the bulk chondrite. The Ge isotopic fractionation, *i.e.*, $\Delta^{74/70}Ge_{bulk\text{-}metal} = \delta^{74/70}Ge_{bulk} - \delta^{74/70}Ge_{metal}$ = –0.03 ± 0.21‰, for the H OC is near zero, compared with $\Delta^{74/70}Ge_{bulk\text{-}silicate}$ = 0.16 ± 0.33‰, $\Delta^{74/70}Ge_{bulk\text{-}sulfide}$ = 1.06 ± 0.16‰, and $\Delta^{74/70}Ge_{metal\text{-}silicate}$ = 0.22 ± 0.36‰ (Table 4; Fig. 4A,B). This indicates that the metal phase was the main contributor to the bulk Ge isotopic budget and that the $\delta^{74/70}Ge_{metal}$ values are a proxy for the $\delta^{74/70}Ge_{bulk}$ values.

In addition, we did not observe any correlation between the degree of shock and germanium isotopic composition. For example, Allegan (H5, S1) and Roses city (H5, S6) had identical $\delta^{74/70}Ge_{bulk}$ isotopic compositions (Table 3).composition.

4. Discussion

4.1. Metal-silicate-sulfide fractionation during condensation

During the cooling of a primordial nebular gas, metal (FeNi) and forsterite (Mg_2SiO_4) condense at similar temperatures, *i.e.*, $T_{50\%\ condensation}$ = 1370K at 10^{-4} atm (Yoneda and Grossman, 1995). The most abundant gaseous molecular species of germanium are GeS, $GeBr_2$, and GeO (Sears, 1978). As $GeBr_2$ is a highly volatile species of Ge, which condenses at much lower temperatures than GeS and GeO (Sears, 1978; Wai and Wasson, 1979; Wood *et al.*, 2019), here, we only discuss GeS and GeO condensation. Condensation of GeS and GeO via reactions with existing silicates and FeNi alloys occur at $T_{50\%\ condensation}$ = 883K (ideal Ge

solution; Lodders *et al.*, 2009) or $T_{50\%\ condensation}$ = 825–830K (no ideal solution; Wai and Wasson, 1977; Wood *et al.*, 2019) and $pH_2O/pH_2 = 4.2 * 10^{-4}$. Sears (1978) showed that Ge is siderophile during high-temperature condensation and becomes lithophile at low temperatures. Thus, germanium condenses first in the metal based on the following reaction (Sears, 1978; Wai and Wasson 1979):

$$GeS_{(g)} + H_2 = Ge_{(s,\ in\ metal)} + H_2S_{(g)}. \quad (2)$$

Then, at lower temperatures, the remaining Ge is incorporated into the silicate phase according to the following reaction (Sears, 1978; Wai and Wasson, 1977):

$$nGeO_{(g)} + 2Mg_2SiO_{4(s)} + H_2O_{(g)} = 2MgSiO_{3(s)} + Mg_2(nGe, 1\text{-}nSi)O_{4(s)} + H_2. \quad (3)$$

On the other hand, sulfide condenses at lower temperatures than metal and silicate ($T_{50\%\ condensation}$ = 691K) via reactions between H_2S_{gas} and solid metal based on the following reaction (Lauretta *et al.*, 1997, and references therein):

$$H_2S_{(g)} + Fe_{(s)} = FeS_{(s)} + H_{2(g)}. \quad (4)$$

The extent and direction of isotopic fractionation in the solid condensate with respect to the vapor source is difficult to evaluate and depends on whether the system maintains equilibrium, is kinetically controlled, or is in a closed or open system. High-temperature equilibrium processes do not induce significant isotopic fractionation, whereas kinetic condensation can result in isotopic fractionation based on the relative cooling rate of the gas and partial pressure of the relevant elements in the gas (Richter, 2004). Calculations from Richter (2004) demonstrate that condensation in an environment, in which the temperature drop is relatively fast compared to the condensation time, results in $P_i << P_{i,sat}$ (where P_i is the partial pressure of a volatile element and $P_{i,sat}$ is its saturation vapor pressure). In this case, kinetic condensation produces a large isotopic fractionation between the source and condensing phase, where the first condensate is enriched in light isotopes. In the condensation sequence, the metal phase that condenses first has the

lightest Ge isotopic composition compared with that of the silicate and sulfide. In contrast, we observed higher $\delta^{74/70}Ge_{metal}$ values for the metal than for the silicate and the lowest $\delta^{74/70}Ge_{sulfide}$ values in the H chondrites (Fig. 3A).

We can draw the same conclusion from the sulfide data. Sulfides in equilibrated OCs are depleted in germanium, with a Ge content as low as 2 ppb and light isotopic composition of $\delta^{74/70}Ge = –1.56‰$ (Fig. 3A). As the first Ge condensates are incorporated into the Fe-Ni alloys, the late sulfide condensate result in (i) a low Ge content (as observed here), despite the fact that Ge is a chalcophile element (Chou *et al.*, 1973), and (ii) a heavier Ge isotopic composition for the sulfides as compared with the metal (Davis and Richter, 2014). The lighter $\delta^{74/70}Ge_{sulfide}$ values compared with the $\delta^{74/70}Ge_{metal}$ values, however, rules out condensation from a protoplanetary disk as a viable process for the origin of Ge isotopic fractionation in metal-silicates and sulfides in ordinary chondrites.

4.2. Evidence for metal-silicate-sulfide partial equilibration before OC accretion

Germanium isotopic compositions in metal, silicate, and sulfide phases in all samples of the H chondrites display the following relationship: $\delta^{74/70}Ge_{sulfide} << \delta^{74/70}Ge_{silicate} < \delta^{74/70}Ge_{meta}$ (Fig. 3A). This relationship holds even for the most reduced type 3 samples, which are the least affected by thermal metamorphism at T<675°C (Tait *et al.*, 2014), which is too low to melt metal or silicate. This observation suggests that the positive $\Delta^{74/70}Ge_{metal\text{-}silicate} = +0.22 \pm 0.36‰$ (varying from +0.17 to +0.33‰ in H3) values is due to metal-silicate exchange that occurred before the accretion of H ordinary chondrite parent body. This positive $\Delta^{74/70}Ge_{metal\text{-}silicate}$ also occurs between the Earth silicate reservoir ($\delta^{74/70}Ge = +0.56 \pm 0.16‰$) and magmatic Fe-meteorites ($\delta^{74/70}Ge = +1.41 \pm 0.22‰$) (Luais, 2012), which may represent the core of early formed planetesimals. Therefore, higher $\delta^{74/70}Ge$ values in metal compared to silicate, in both

undifferentiated and differentiated bodies, appears to be the result of metal-silicate equilibrium. The larger $\Delta^{74/70}Ge_{metal\text{-}silicate}$ of +0.85‰ in differentiated bodies reservoirs (e.g. the silicate Earth and Fe- meteorites, Luais, 2012) compared to $\Delta^{74/70}Ge_{metal\text{-}silicate}$ in OCs can reflect additional isotopic fractionation during core-mantle differentiation.

The addition of sulfur in the Fe-Ni system strongly modifies the Ge incorporation into the metal phase. Chabot *et al.* (2003) and Chabot and Jones (2003) demonstrated that, during fractional crystallization at FeNi-S metallic liquid equilibrium, the $D(Ge)_{solid\ metal/liquid\ metal}$ value increases by several orders of magnitude as S increases in the liquid. Similar low Ge contents have also been observed in S-rich melts during Fe-Ni-S partial melting experiments (Rushmer *et al.*, 2005). Low Ge contents (2 ppb) in sulfide from type 4 and 6 OCs (Fig. 3A) likely result from late-stage fractional crystallization of Fe-Ni-S melts. The strongly negative $\delta^{74/70}Ge_{sulfide}$ value of –1.56‰ appears to be a feature common to sulfides formed by fractional crystallization, such as terrestrial sulfides (Belissont *et al.*, 2014). As we have no isotopic values for the H3 type, it is unclear if sulfide crystallization occurs during nebular processes or on the parent body. However, the discrepancy between temperatures associated with the H4 petrologic type (676–865°C; Tait *et al.*, 2014) and FeNi-S fusion temperature (963°C; Mare *et al.*, 2014) suggest that negative Ge isotopic composition of sulfides could have been inherited from processes that occur before parent body accretion, as it has been proposed for metal and silicate phases.

Equilibrium among metal, silicate, and sulfide in ordinary chondrites must then reflect processes before the accretion, such as (1) partial re-equilibration of material produced by disruption of partially differentiated planetesimals, or (2) a heating event in the solar nebula. Bischoff *et al.* (2018) reported that, in more than 2280 polished OC thin sections, there was a high abundance of brecciated rocks and occurrences of xenolithic fragments (*e.g.*, CI, CM, and Ureilite) in type 3 OCs. This supports the hypothesis that OCs can represent aggregates of early formed achondritic, chondritic, and chondrule materials. Lichtenberg *et al.* (2018) argued that

OC parent bodies can form from early impact on a preheated (*i.e.,* ^{26}Al decay) and partially differentiated planetesimal (Bryson et al. 2019). Thus, the negative $\delta^{74/70}$Ge values of the bulk sample and all separated OC phases, compared with positive values for magmatic iron meteorites and Earth silicate reservoirs, imply a light isotope-enriched environment for OC formation, *i.e.*, an impact plume environment. Evaporation processes that occur during an impact would likely overprint any $\Delta^{74/70}Ge_{metal\text{-}silicate}$ signature from a previous generation of planetesimals. Metal, metal-silicate, and sulfide would partially re-equilibrate after this event during partial melting in a gas enriched in light Ge isotopes. This model of metal melting before OC accretion agrees with a recent study of metal formation in L OCs (Okabayashi *et al.*, 2019).

4.3. Post accretional processes

4.3.1. No shock effect on $\delta^{74/70}Ge_{metal}$ and $\delta^{74/70}Ge_{bulk}$ values

As the germanium is a moderately volatile element, evaporation should result in a significant enrichment in heavy isotopes in highly shocked samples. The H chondrite Roses City, an impact melt breccia (S6), shows no deviation in $\delta^{74/70}Ge_{metal}$ from the mean values for H group while Dhajala (S1) is enriched in heavy isotopes compared with other H chondrites. Similarly, for L group samples, there is no $\delta^{74/70}Ge_{metal}$ difference between highly shocked (Alfianello and Vouillé, both S5) and minimally shocked samples (Björbole, S1). The lack of a shock effect on the $\delta^{74/70}$Ge values can be explained by the deep burial of material, which should inhibit light isotope evaporation due to the pressure (*e.g.*, Roses City, H5), or an increase in temperature during a low energetic impact, which may be not sufficient to efficiently evaporate Ge.

4.3.2. Effects of metamorphism

Unequilibrated OCs (type 3) are primitive and may correspond to the outer layer of a layered planetesimal (Trieloff *et al.*, 2003) that experienced low-temperature metamorphic processes (< 675°C; Tait *et al.*, 2014). They represent the most reduced type of each OC group (Rubin, 2005). This implies that metal-silicate exchange is limited compared to other petrologic types and that younger processes may not have overprinted isotopic fractionation, which had been established before planetesimal accretion (Van Schmus and Wood, 1967).

From the H3 to H5 petrologic types, certain variations in the $\Delta^{74/70}Ge_{\text{metal-silicate}}$ values (Fig. 4B) indicate Ge isotopic exchange between metal and silicate during thermal metamorphism. However, the lack of variation in the $\delta^{74/70}Ge_{metal}$ values suggests that metamorphism had no measurable effect on the Ge isotopic composition of the metal phase. Thus, variations in the $\Delta^{74/70}Ge_{\text{metal-silicate}}$ values (Fig. 4B) indicate an increased sensitivity to $\delta^{74/70}Ge_{silicate}$ during metamorphic processes due to the lower Ge content in the silicate compared to the metal. Melting points for the FeNi-S assemblage and silicate are 963°C and 1050°C, respectively, at 0.3 kBar (Mare *et al.*, 2014 and references therein). Types 3 to 5 OCs experienced different peak metamorphism temperatures from T < 675°C for H3, 525–727°C for H4, and 676°C < T < 865°C for H5 (Monnereau *et al.*, 2013; Tait *et al.*, 2014). These temperature ranges are likely too low to melt FeNi-S alloy and cause metal-silicate exchange. In contrast, type 6 OCs reached temperatures between 866°C and 1000°C (Monnereau *et al.*, 2013; Tait *et al.*, 2014). FeNi-S melting and efficient Ge silicate-metal exchange resulted in an increase in the Ge content for metals from the H3–H5 types ($[Ge]_{mean}$ = 61.9 ppm), excluding Allegan (see section 3.1), to the H6 type ($[Ge]_{mean}$ = 66.0 ppm), which agrees with Ge diffusion from silicate to metal during metamorphism (Chou *et al.*, 1973). Similarly, Ge isotopic exchange between metal and silicate in H6 resulted in a heavier silicate isotopic composition, which approached the isotopic composition of the metal. This led to a similar Ge isotopic composition for the silicate, metal, and bulk in the H6 chondrites within the 2σ error range (Fig. 4A,B).

The global scheme for L chondrites is not as clear as it is for H chondrites. Except for the Bjürbole sample (L4 at –0.5‰), silicates from the L6 chondrites have negative and heterogeneous $\delta^{74/70}$Ge values that are distinct from the metal phase values (Figure 3A), which suggest that there was no isotopic re-equilibration, such as that observed in H6 chondrites. The "onion shell" model is less constrained for L chondrites. Göpel *et al.* (1994) proposed that the L parent body formed from thermal gradient disruption due to impact processes and reassembly. If this had occurred before metal-silicate equilibration, this could have prevented the efficient Ge exchange between the metal and silicate. Finally, the isotopic uniformity of the metal phases from H3 to H6 and L3 to L6 (Figure 2B) are consistent with closed-system metamorphism within each parent body.

4.4. Links between the redox process and $\delta^{74/70}$Ge variations throughout the H–L–LL sequence

The main characteristic of ordinary chondrites is their increase in oxidation state through the H, L, and LL sequences, which is inferred from the decrease in metal content and increase in the percentage of fayalite in olivine (Chou *et al.*, 1973). The similar increase in the δ^{18}O composition and Δ^{17}O anomalies from the H to LL OCs (Clayton *et al.* 1991) led Rubin (2005) to identify a correlation between the % Fa in olivine and the δ^{18}O and Δ^{17}O values.

The Ge concentration and isotopic composition in metal increases from the H to L to LL groups (Fig. 2B), which discounts the occurrence of any Ge loss and evaporative processes during OC formation. A well-defined positive correlation was identified among the %Fa, Ge concentrations, and $\delta^{74/70}$Ge in metal for all petrographic types and groups (Fig. 5A and B). At first glance, this suggests that the metal becomes enriched in Ge and the heavy isotopes of Ge with increasing oxidation. However, as the D(Ge) value decreases with an increasing fO_2 (Kegler and Holzheid, 2011), we can expect the metal in the L chondrites to become depleted in Ge

compared to the metal in H chondrites, whereas we observe the opposite (Fig. 5). Therefore, oxidation is not the main process that causes an increase in Ge content from H to LL. In the Urey and Craig-type diagram, *i.e.*, $Fe_{metal + sulfide}$ vs FeO (Krot *et al.*, 2014), variations in reduced Fe and FeO do not follow the reduction-oxidation trend, suggesting that the system has lost some of its iron metal. In this case, the increase in the Ge content for the metal from H to LL, with a broadly constant Ge bulk concentration (Wasson and Kallemeyn, 1988), can be explained by the incorporation of Ge into the remaining metal. However, this process cannot explain the increase in the $\delta^{74/70}$Ge throughout the OC sequence. In conclusion, the increases in Ge, $\delta^{74/70}$Ge, and %Fa are not related to oxidation conditions in the environment of OC formation, *i.e.*, the fO_2 conditions. One explanation may be the involvement of an oxidizing component

The $\delta^{74/70}$Ge values and δ^{18}O and Δ^{17}O are also characterized by a positive correlation (Fig. 6) in which these three groups are distinguishable outside of the analytical errors, with the following values for H (mean Δ^{17}O = 0.71 ± 0.12‰ and $\delta^{74/70}$Ge = –0.51 ± 0.09‰), L (mean Δ^{17}O = 1.02 ± 0.15‰ and $\delta^{74/70}$Ge = –0.31 ± 0.06‰), and LL chondrites (mean Δ^{17}O = 1.18 ± 0.12‰ and $\delta^{74/70}$Ge = –0.26 ± 0.09‰). As metamorphism does not modify $\delta^{74/70}$Ge in metal and bulk chondrite, we suggest that Ge isotopic variations among the three groups are the result of accretionary processes. Hence, correlations among [Ge]-$\delta^{74/70}$Ge-%Fa, δ^{18}O, and Δ^{17}O reflect processes that originated in the accretionary disk, which were broadly linked to the redox state. Specifically, chondrule mixing of type I-reduced and type II metal-free chondrules (Clayton *et al.*, 1991, Zanda *et al.*, 2006), as well as the incorporation of an oxidizing component during OC accretion (Rubin, 2005) were the two main processes (see discussion below).

4.4.1. Chondrules as carriers of a high $\delta^{74/70}$Ge signature?

Clayton *et al.* (1991) demonstrated that, in certain ordinary chondrites, small-size chondrules (with diameter d < 300 µm) show enrichment in ^{16}O and depletion in ^{17}O compared with larger chondrules (d > 300 µm). This difference has been interpreted in terms of the interaction between ^{16}O-poor melted chondrules and ^{16}O-rich gas at their time of formation. Chondrules were then classified into type I chondrules (magnesian), which are small, reduced, metal-rich, and depleted in volatiles, and type II chondrules (ferroan), which are larger, oxidized, metal-free, and volatile-rich (Zanda, 2004; Zanda *et al.*, 2006). Additionally, Zanda *et al.* (2006) showed that the proportions of the type I chondrule decrease through the OC sequence while type II increases (type I: 45%, 28%, and 22%; type II: 36%, 58%, and 61% in the H, L, and LL groups, respectively). Based on the sizes of type I and II chondrules, their volume in the H, L, and LL OCs, and the oxygen isotopic compositions of large chondrules (heaviest) compared to small chondrules, Clayton *et al.* (1991) argues that the increase in $\Delta^{17}O$ through the H-L-LL sequence can be explained by a "size-sorting process" of chondrules, whereas Zanda *et al.* (2006) argue for mixing between petrological components of the chondrites. Thus, considering the $\delta^{74/70}Ge$-$\delta^{18}O$-$\Delta^{17}O$ correlations (Fig. 6 and 7), we can assess if type II chondrules have a heavier $\delta^{74/70}Ge$ composition compared with type I chondrules. An increase in type II can elevate the $\delta^{74/70}Ge$ ratio in type II rich-ordinary chondrites.

We used two approaches to test the chondrule mixing hypothesis. First, we calculated the inferred $\delta^{74/70}Ge$ composition of type I and type II chondrules, as well as the matrix, to account for variations in $\delta^{74/70}Ge$ from H to LL due to mixing between these components (Fig. 7A). This mass balance calculation is based on Zanda *et al.* (2006), with type I and II chondrules, the matrix proportions in H, L, and LL, and their respective oxygen isotopic compositions (see the caption for Fig. 7 for more details and Table 2 in Zanda *et al.* 2006). Based on this modeling, we obtained the following theoretical compositions: $\delta^{74/70}Ge_{type\ I}$ = –0.81‰, $\delta^{74/70}Ge_{type\ II}$ = 2.15‰, and $\delta^{74/70}Ge_{matrix}$ = –7.35‰.

For the second approach, we analyzed the Ge isotopic composition of type I and II chondrules. As it is not possible to distinguish between type I and II chondrules at the macroscopic scale, we used the same protocol as Clayton *et al.* (1991) on the same meteorite (Dhajala H3.8). We separated two chondrule fractions (*i.e.*, d < 300 and d > 300 µm) based on the assumption that the smaller fraction should be mainly composed of type I chondrules while the larger fraction contains type II chondrules. Our results on the chondrule fractions show that the $\delta^{74/70}$Ge values of small ($\delta^{74/70}Ge_{d<300\mu m}$ = –0.28 ± 0.12‰) and large chondrules ($\delta^{74/70}Ge_{d>300\mu m}$ = –0.38 ± 0.11‰) (Table 3) are similar within error and are near the Dhajala bulk value ($\delta^{74/70}$Ge = –0.37 ± 015‰). In the $\delta^{74/70}$Ge-δ^{18}O diagram, the graphic, Dhajala bulk chondrite plots on the mixing line defined by type I and II Dhajala chondrules, indicating no analytical artefact. However, type I and II chondrule isotopic compositions do not plot on the $\delta^{74/70}$Ge-δ^{18}O OC mixing line (Fig. 7B) and do not agree with the calculated values for type I and II chondrules. This precludes any mixing process between type I and II chondrules that can explain the H, L, and LL correlation.

An *in-situ* ion probe study of oxygen isotopes in individual olivine and pyroxene phases of OC chondrules yielded a more complex picture. Variable δ^{18}O but similar Δ^{17}O values have been found in type I and II chondrules from H chondrites, as well as the Semarkona (LL3) chondrite (Kita *et al.*, 2010). In Semarkona, type I and II chondrules both have similar Δ^{17}O values (+0.5–0.7‰) that are lower than bulk LL chondrites (+1.2‰), indicating that chondrule phenocrysts do not host the Δ^{17}O anomalies. Thus, the issue is not the dichotomy between the O isotopic compositions of type I and II chondrules but the recognition of a high Δ^{17}O anomaly. For example, a previous study has found a Δ^{17}O anomaly in chondrule glass from the LL chondrite, which resulted from aqueous alteration with a high Δ^{17}O ice component (Kita *et al.*, 2010). Germanium isotopes and detailed studies of O anomalies in chondrules do not favor a mixing model that links phenocrysts in type I and II chondrules with the redox state but mixing with, or

incorporation of, a high $\Delta^{17}O$ oxidized component in the chondrules or chondrite matrix is a viable model. The similar Ge isotopic composition between the type I and II chondrules suggests that evidence of an oxidizing component with high $\Delta^{17}O$ must occur in the matrix of ordinary chondrites. A systematic investigation of the Ge isotopic compositions of chondrules and the matrix of the H, L, and LL types is necessary to understand similarities in their composition.

4.4.2. $\delta^{74/70}Ge$- $\Delta^{17}O$-%Fa correlations in OCs and accretion of hydrated phyllosilicate

The main issue with the correlation between Ge elemental/isotopic variations in ordinary chondrites and %Fa in olivine, as well as between $\delta^{18}O$ and the $\Delta^{17}O$, is the origin of oxidation and how it relates to asteroidal processes and/or a nebular origin.

Clayton and Mayeda (1988) first identified the correlations between %Fa in olivine and $\delta^{18}O$ and $\Delta^{17}O$ in Urelites. They interpreted these correlations to be associated with oxidation processes in the nebula. Similarly, Rubin (2005) highlighted the $\Delta^{17}O$-%Fa positive correlation among OC groups, suggesting that the increase in the oxidation state through the OC sequence is related to an increase in the proportion of an accreted oxidizing agent with high $\delta^{17}O$, $\delta^{18}O$, and $\Delta^{17}O$ signatures. Choi *et al.* (1998) identified such elevated oxygen isotopic signatures in magnetite from unequilibrated LL OCs, which show a large and unusual deviation from the Terrestrial Fractionation Line (TFL; $\Delta^{17}O \approx 5‰$) compared with OCs that have typical values ($\Delta^{17}O \approx 0$ to 2‰). Choi *et al.* (1998) suggested that high ^{18}O-nebular water ($\delta^{18}O = 21‰$ and $\Delta^{17}O \approx 7‰$) accreted onto the OC parent body and induced low-temperature aqueous alteration. Such asteroidal alteration was responsible for the formation of magnetite via FeNi alloy oxidation (Wasson and Krot, 1994; Krot *et al.*, 1997; Choi *et al.*, 1998), the growth of fayalite rims on pyroxene grains via reactions between oxidized Fe and silica (Wasson and Krot, 1994), and the

presence of phyllosilicates in LLs and unequilibrated OCs (Hutchison *et al.*, 1987; Choi *et al.*, 1998).

Attributing the high Ge-$\delta^{74/70}$Ge compositions to the high ^{18}O-nebular component (Figs. 5 and 6) and the main oxidizing agent in the low temperature (T < 500K) nebula to an H_2O-gaseous component (McSween and Labotka, 1993; Krot *et al.*, 1997) is tempting. However, there is a large debate on the thermodynamic state of H_2O. McSween and Labotka (1993) and Krot *et al.* (1997) have proposed that ice condensate in the nebula accreted to OC parent bodies, and, then, later heated to form vapor during metamorphism and reacted to form phyllosilicates, such as described in the LL3 unequilibrated chondrites. Wasson and Krot (1994) and Wasson (2000) argued that the low temperatures, *i.e.*, 160 K (or at 182 K; Lodders *et al.*, 2009), required to condensate ice cannot be attained in the nebular locations that form OCs (within 2–3 AU). Instead, they have suggested that H_2O derived from accreted hydrated silicates. Here, the key issue is how germanium can be incorporated into the low-temperature H_2O-oxidizing component. At germanium condensation temperature ($T_{50\%}$ cond) of 875K at 10^{-4} atm, Ge may have already condensed, and low-temperature ice condensates likely do not contain much Ge. However, hydrated silicates that form at the end of the condensation sequence but at higher temperatures than ice ($T_{50\%}$ cond < 350°C; Grossman and Larimer, 1974) can contain small amounts of Ge. Therefore, one possibility is that dust enrichment in the continuously accreting nebula can yield higher $T_{50\%}$ condensation (Wasson, 2000; Davis and Richter, 2014). We propose that the last fraction of Ge, likely in the form of $GeBr_2$ (the second Ge most abundant species of Ge specie in the solar nebula, which is highly volatile; Sears, 1978), can condense in phyllosilicates and acquire the high $\delta^{74/70}$Ge values discussed in section 4.1

We have modelled the mixing between bulk H chondrite and the oxidizing phyllosilicate (Fig. 8) to (1) reproduce the OCs correlation in Figure 6 and, (2) determine what percentage of

accreted phyllosilicate is needed to change the composition from H to LL chondrites in terms of Ge content and $\delta^{74/70}$Ge in phyllosilicate. To constrain the model, we have considered the amount of accreted phyllosilicate, which cannot be higher than the amount of matrix (<15%, Krot *et al.*, 2014), and the Ge content in terrestrial phyllosilicates. This value ranges between 1.1 – 8.5 ppm with means of 3.8 ± 3.2 ppm (2σ SD, calculated from Bernstein, 1985, and references therein). The model shows that at Ge content of 3.8 ± 3.2 ppm and ~10 to 15% of accreted phyllosilicate, a composition from $\delta^{74/70}$Ge = +6‰ to +3.2‰, respectively, is needed to change the isotopic composition from H to LL. By extrapolation of the $\delta^{74/70}$Ge-Δ^{17}O correlation shown in Figure 6, we find that the $\delta^{74/70}$Ge = 3.2 – 6‰ in phyllosilicates would correspond to a Δ^{17}O ≈ +8 to +15‰. The lower Δ^{17}O is close to the value of the oxidized nebular component incorporated in OC parent bodies reported by Choi *et al.* (1998) (Δ^{17}O ≈ +7‰), yet a better match is attained for a $\delta^{74/70}$Ge = +2.5‰ (Δ^{17}O = +7‰) in phyllosilicates. This value implies a Ge content of about 4.8 to 7 ppm for 15% and 10% of phyllosilicate, respectively. So, it seems possible that phyllosilicates could contain between 4 to 7 ppm of Ge with a composition of $\delta^{74/70}$Ge ≈ +3 to +2.5‰. It can be noted that a Ge content in phyllosilicates of few ppm is likely from the thermodynamic calculation (Sears, 1978). They predict that a significant proportion of Ge (in the form of $GeBr_2$) would remain in the gas even after troilite condensation and that Ge would become lithophile at the end of the condensation sequence (Sears, 1978).

During planetesimal heating, the dehydration of accreted phyllosilicates triggers a redox reaction on the parent body. The release of ^{18}O-rich and $\delta^{74/70}$Ge-high water (or vapor) oxidizes the Fe-Ni metal as FeO, forming magnetite, which then increases the %Fa in olivine. Germanium released in water is likely incorporated in the metal due to its siderophile behavior. However, the small amount of Ge does not contribute to the significant increase in Ge from the H to L to LL OCs. In contrast, the high $\delta^{74/70}$Ge composition of the released H_2O component that reacted with the metal should have significantly increased the $\delta^{74/70}Ge_{metal}$ proportional to the

amount of accreted oxidizing agent on each OC parent body. As such interaction may occur during metamorphism, a correlation for the $\delta^{74/70}Ge_{metal}$ composition is possible for types 3 to 6 in a given OC group. However, we propose that the lack of a $\delta^{74/70}Ge_{metal}$ correlation with the petrologic type is imputable to the relatively high temperature of thermal metamorphism, which is even recorded in the earlier stage of pervasive H_2O alteration via magnetite formation in the type 3 chondrite (T < 675°C) (Krot *et al.* 1997; Choi *et al.*, 1998; Tait *et al.*, 2014). The fractionation of stable isotopes at equilibrium is a function of $1/T^2$, such that an increase in the metamorphic temperature from types 3 to 6 (T < 675 to 975°C, Tait *et al.*, 2014) does not induce significant variations in the Ge isotopic fractionation between the H_2O-component and metal with the petrologic type. Hence, the observed Ge isotopic fractionation among groups is primarily a function of the amount of nebular hydrated phyllosilicate with a high $\delta^{74/70}Ge$ signature accreted onto the parent body. The heavy O isotopic composition of OCs that partly derive from phyllosilicate destabilization can be considered, along with the previous H_2O gas or ice model for the origin of accreted water.

4.5. Dhajala: A reduced L chondrite

The higher $\delta^{74/70}Ge_{metal}$ composition of Dhajala (H3.8) compared with the other H chondrites, including Sharps (H3.4), which has a similar petrologic type, requires discussion because Dhajala does not fit the correlations shown in Figs. 5B and 6. Dhajala and Sharps have both experienced a low degree of metamorphism. They lie within the oxygen isotope field as H chondrites but Dhajala (H3.8) has oxygen isotopic anomalies that are slightly higher than Sharps (H3.4) ($\Delta^{17}O_{Dhajala}$ = 0.698 ‰and $\Delta^{17}O_{Sharps}$ = 0.646 ‰; Clayton *et al.*, 1991). The high Fe_{metal} (15.98 wt. %), and low FeO_{bulk} (10.18 wt. %) contents in Dhajala compared with Sharps (Fe_{metal} = 12.02 wt. % and; FeO_{bulk} = 13.64 wt. %) (Table 5) reflect more reduced conditions for Dhajala than for Sharps. In contrast, the high percentage of fayalite and low carbon content in Dhajala

(%Fa = 19.3; C = 0.04 wt. %) indicate more oxidized conditions than for Sharps (%Fa = 17.5 and C = 0.95 wt. 95 wt. %) (Jarosewich, 1990). In addition, the Dhajala germanium isotopic composition is closer to L type composition than H type (Figs. 2 and 6). Thus, we propose that Dhajala accreted identical proportions of oxidizing component than L chondrites, which led to olivine formation with high %Fa (> 20) and an increase in the $\delta^{74/70}Ge_{metal}$ composition that approaches the L Ge isotopic signature. Dhajala then experienced reduction by carbon (McSween and Labotka, 1993) based on the following reaction (Warren and Huber, 2006):

$$C + MgFeSiO_4 = MgSiO_3 + Fe + CO. \quad (5)$$

In conclusion, the elevated $\delta^{74/70}Ge_{metal}$ composition in Dhajala with low %Fa is the result of high carbon activity in this meteorite, which did not decrease due to C dissolution in taenite (Romig and Goldstein, 1978) by contrast with Sharps. This implies that Dhajala most likely formed in the L region of the accretionary disk before reduction via carbon. This suggests that the OC accretion environment is heterogeneous and $\delta^{74/70}Ge$ should be considered a tracer of the primary locations that formed undifferentiated meteorites.

4.6. Relationship between the OC redox state and IIE iron meteorites

IIE non-magmatic iron meteorites formed by impact-induced melting and the destruction of a chondritic parent body, followed by metal silicate re-accretion (Luais, 2007*;* Ruzicka, 2014; Wasson and Wang 1986). This group can be divided into old (Miles, Weekeroo Station) and young groups (Netschaëvo, Watson), which formed from 4.3 – 4.5 and 3.5 – 3.8 Ga, respectively (Bogard *et al.*, 2000). They have a complex mineralogy, mainly composed of metal and silicate inclusions. These inclusions represent 5 to 10 vol. % of the IIE meteorites and are composed of silicates (feldspar, pyroxene, and olivine) phosphates, sulfides, and chromite (McDermott *et al.*,

2016). Silicate inclusions can be classified into two categories, chondritic inclusions with relic chondrules and differentiated inclusions (McDermott *et al.*, 2016).

The genetic links between the H OC and IIE iron meteorites were first identified based on the similar elemental and oxygen isotopic compositions of silicate inclusions from IIE iron and silicates from the H OC (Olsen and Jarosewich, 1971; Clayton and Mayeda, 1996). However, based on the (1) concentrations in the refractory and volatile siderophile elements and (2) low $\Delta^{17}O$ values in silicate inclusions in the IIE Netschaevo meteorite, we can infer that the impact, which formed the IIE iron meteorites, occurred on an HH parent body that was more reduced than the H group (McDermott *et al.*, 2016; Wasson, 2017).

To study the genetic link between the IIE irons and OCs, we only must consider meteorite samples from the IIE old group because they display the most pristine $\delta^{74/70}Ge_{metal}$ compositions compared with the young group, which show an increase in $\delta^{74/70}Ge_{metal}$ due to successive impacts (Luais, 2007). Figure 9 shows the positive correlation among the $\delta^{74/70}Ge$ composition of IIE bulk metal (Luais, 2007; Luais, 2012), OC metal (data from this study), and $\Delta^{17}O$ measured in silicate inclusions from IIE irons and bulk silicates from the H, L, and LL OCs (see Table 5 for oxygen references). IIE iron meteorite values for $\delta^{74/70}Ge_{metal}$ and $\Delta^{17}O_{silicate\ inclusions}$ are lower than those for the H chondrites. As the H chondrites are the less oxidized group, the lower $\delta^{74/70}Ge_{metal}$ and $\Delta^{17}O_{silicate\ inclusion}$ values (Fig. 9) of the IIE old groups compared to the H group, correspond to the isotopic composition of the most reduced HH parent body. Germanium isotopes demonstrate that there is a genetic link between the IIE iron meteorites and HH parent body.

5. Summary

We report the first data set of germanium isotopic compositions for bulk and separated phases from ordinary chondrites. The Germanium isotopic compositions were measured by an MC-ICP-MS coupled to a hydride generator system with a 2σ long term reproducibility of 0.1‰. We found that the Ge isotopic composition of ordinary chondrites is mainly driven by the metal phase, which is a good proxy for the OC bulk composition. The $\delta^{74/70}Ge_{metal}$ values significantly increased throughout the OC sequence, such that H, L, and LL groups are distinguishable at –0.51 ± 0.09‰, –0.31 ± 0.09‰, and –0.26 ± 0.09‰, respectively. The implications of the germanium isotopic compositions for the understanding of ordinary chondrite compositions can be summarized as follows.

- The lack of significant $\delta^{74/70}Ge_{metal}$ variation between the unequilibrated and equilibrated OCs within each group implies that $\delta^{74/70}Ge$ variation among groups is inherited from nebular processes rather than parent body processes.
- Metal and silicate are partially equilibrated in a closed system during metamorphism.
- The positive $\Delta^{74/70}Ge_{metal\text{-}silicate}$ signature is remarkably similar to previously reported Ge isotopic fractionations between magmatic iron meteorites and Earth silicates. However, the light $\delta^{74/70}Ge$ composition of both metal and silicate suggests that metal, silicate, and sulfide have interacted before the accretion of ordinary chondrite parent bodies in a gas enriched in light Ge isotopes.
- The two well-defined positive correlations between $\delta^{74/70}Ge_{metal}$ and %Fa, as well as $\Delta^{17}O$, demonstrate that the Ge isotopic composition can be used as a tracer of oxidizing processes during accretion. The similar Ge isotopic compositions of small and large chondrules (from Dhajala) indicate that the size sorting chondrule mechanism cannot account for the $\delta^{74/70}Ge_{metal}$-%Fa and $\Delta^{17}O$ correlations. Therefore, these correlations can be explained by an increase in the amount of accreted high $\Delta^{17}O$ hydrated nebular phyllosilicates with high $\delta^{74/70}Ge$ of about 2.5 to 3 ‰, throughout the ordinary chondrite

sequence. We can reconsider the origin of the heavy O isotopic signature in ordinary chondrites to derive from either H_2O (water) or hydrated silicate.

- The $\delta^{74/70}Ge_{metal}$-$\Delta^{17}O_{silicate}$ correlation in the OCs provides evidence for the existence of an HH reduced parent body and its genetic link with the IIE iron meteorites.

Acknowledgments

The authors thank Damien Cividini for his valuable assistance on the Neptune*Plus* MC-ICP-MS and his advice on germanium chemistry, and Delphine Yeghicheyan (SARM "Service d'Analyses des Roches et des Minéraux", CRPG-CNRS, Nancy) for contribution to elemental analyses. The authors also acknowledge Andreas Pack for oxygen isotopic measurements. We thank M. Gounelle and the "Comité de gestion" at the "Muséum National d'Histoire Naturelle" (MNHN) of Paris, T. McCoy and J. Hoskin from the Smithsonian Institute, and A. Nieto Codina from the "Museo Nacional de Ciencias Naturales" (MNCN) of Madrid for providing the meteorite samples. Jesse Davenport is thanked for his kind and careful correction of the manuscript. Finally, we thank Fang Huang for editorial handling, and three anonymous reviewers for their thorough and constructive reviews that helped to improve the manuscript. This is CRPG contribution n°2724.

Research Data

Research Data associated with this article can be access at https://doi.org/10.17632/5rfdtkx27w.1

References

Abdul-Majeed W. S. and Zimmerman W. B. (2012) Computational Modelling of the Hydride Generation Reaction in a Tubular Reactor and Atomization in a Quartz Cell Atomizer. *JASMI* **02**, 126–139.

Archer G. J., Walker R. J., Tino J., Blackburn T., Kruijer T. S. and Hellmann J. L. (2019) Siderophile element constraints on the thermal history of the H chondrite parent body. *Geochim. Cosmochim Acta* **245**, 556-576.

Belissont R., Boiron M.-C., Luais B. and Cathelineau M. (2014) LA-ICP-MS analyses of minor and trace elements and bulk Ge isotopes in zoned Ge-rich sphalerites from the Noailhac – Saint-Salvy deposit (France): Insights into incorporation mechanisms and ore deposition processes. *Geochim. Cosmochim. Acta* **126**, 518–540.

Bennett M. E. and McSween H. Y. (1996) Shock features in iron-nickel metal and troilite of L-group ordinary chondrites. *Meteorit. Planet. Sci.* **31**, 255–264.

Bernstein L. R. (1985) Germanium geochemistry and mineralogy. *Geochim. Cosmochim. Acta* **49**, 2409–2422.

Bischoff A., Schleiting M., Wieler R. and Patzek M. (2018) Brecciation among 2280 ordinary chondrites – Constraints on the evolution of their parent bodies. *Geochim. Cosmochim. Acta* **238**, 516–541.

Bogard D. D., Garrison D. H. and McCoy, T. J. (2000) Chronology and petrology of silicates from IIE iron meteorites: evidence of a complex parent body evolution. *Geochim. Cosmochim. Acta* **64(12)**, 2133-2154.

Bryson J. F. J., Weiss B. P., Getzin B., Abrahams J. N. H., Nimmo F. and Scholl A. (2019) Paleomagnetic evidence for a partially differentiated ordinary chondrite parent asteroid. *J. Geophys. Res. Planets* **124(7)** 1880-1898

Budde G., Burkhardt C., Brennecka G. A., Fischer-Gödde M., Kruijer T. S. and Kleine, T. (2016) Molybdenum isotopic evidence for the origin of chondrules and a distinct genetic heritage of carbonaceous and non-carbonaceous meteorites. *Earth Planet. Sc. Lett.* **454**, 293-303.

Burkhardt C., Kleine T., Oberli F., Pack A., Bourdon B. and Wieler R. (2011) Molybdenum isotope anomalies in meteorites: constraints on solar nebula evolution and origin of the Earth. *Earth Planet. Sc. Lett.* **312(3-4)**, 390-400.

Chabot N. L., Campbell A. J., Jones J. H., Humayun M. and Agee C. B. (2003) An experimental test of Henry's Law in solid metal-liquid metal systems with implications for iron meteorites. *Meteorit. Planet. Sci.* **38**, 181–196.

Chabot N. L. and Jones J. H. (2003) The parameterization of solid metal-liquid metal partitioning of siderophile elements. *Meteorit. Planet. Sci.* **38**, 1425–1436.

Choi B.-G., McKeegan K. D., Krot A. N. and Wasson J. T. (1998) Extreme oxygen-isotope compositions in magnetite from unequilibrated ordinary chondrites. *Nature* **392**, 577–579.

Chou C.-L., Baedecker P. A. and Wasson J. T. (1973) Distribution of Ni, Ga, Ge and Ir between metal and silicate portions of H-group chondrites. *Geochim. Cosmochim. Acta* **37**, 2159–2171.

Chou C.-L. and Cohen A. J. (1973) Gallium and germanium in the metal and silicates of L- and LL-chondrites. *Geochim. Cosmochim. Acta* **37**, 315–327.

Clayton R. N. and Mayeda T. K. (1988) Formation of ureilites by nebular processes. *Geochim. Cosmochim. Acta* **52**, 1313–1318.

Clayton R. N. and Mayeda T. K. (1996) Oxygen isotope studies of achondrites. *Geochim. Cosmochim. Acta Acta* **60**, 1999–2017.

Clayton R. N., Mayeda T. K., Goswami J. N. and Olsen E. J. (1991) Oxygen isotope studies of ordinary chondrites. *Geochim. Cosmochim. Acta* **55**, 2317–2337.

Davis A. M. and Richter F. M. (2014) 1.10 - Condensation and Evaporation of Solar System Materials. In *Treatise on Geochemistry (Second Edition)* (eds. H. D. Holland and K. K. Turekian). Elsevier, Oxford. pp. 335–360.

Dedina J. and Tsalev D. L. (1995) *Hydride generation, atomic absorption spectrometry*., Wiley, Chichester (UK).

Dodd R. T. (1968) Recrystallized chondrules in the Sharps (H-3) chondrite. *Geochim. Cosmochim. Acta* **32**, 1111–1120.

Dodd R. T. and Jarosewich E. (1979) Incipient melting in and shock classification of L-group chondrites. *Earth Planet. Sc. Lett.* **44**, 335–340.

Dunn T. L., McCoy T. J., Sunshine J. M. and McSween Jr, H. Y. (2010) A coordinated spectral, mineralogical, and compositional study of ordinary chondrites. *Icarus* **208(2)**, 789-797.

El Korh A., Luais B., Boiron M.-C., Deloule E. and Cividini D. (2017) Investigation of Ge and Ga exchange behaviour and Ge isotopic fractionation during subduction zone metamorphism. *Chem. Geol.* **449**, 165–181.

Elkins-Tanton L. T., Weiss B. P. and Zuber M. T. (2011) Chondrites as samples of differentiated planetesimals. *Earth Planet. Sc. Lett.* **305**, 1–10.

Escoube R., Rouxel O. J., Luais B., Ponzevera E. and Donard O. F. X. (2012) An Intercomparison Study of the Germanium Isotope Composition of Geological Reference Materials. *Geostand. Geoanal. Res.* **36**, 149–159.

Folco L., Bland P. A., D'Orazio M., Franchi I. A., Kelley S. P. and Rocchi S. (2004) Extensive impact melting on the H-chondrite parent asteroid during the cataclysmic bombardment of the early solar system: Evidence from the achondritic meteorite Dar al Gani 89611Associate editor: W. U. Reimold. *Geochim. Cosmochim. Acta* **68**, 2379–2397.

Fouché K.F. and Samles A.A. (1966) The distribution of trace elements in chondritic meteorites. 1. Gallium, Germanium and Indium. *Chem. Geol.* **2**, 5-33.

Göpel C., Manhès G. and Allègre C. J. (1994) U/Pb systematics of phosphates from equilibrated ordinary chondrites. *Earth Planet. Sc. Lett.* **121**, 153–171.

Grossman L. and Larimer J. W. (1974) Early chemical history of the solar system. *Rev. Geophys.* **12**, 71.

Grossman J. N. and Zipfel J. (2001) The Meteoritical Bulletin, No. 85, 2001 September. *Meteorit. Planet. Sci.* **36**, A293–A322.

Guignard J. and Toplis M. (2015) Textural properties of iron rich phases in H ordinary chondrites and quantitative links to the degree of thermal metamorphism. *Geochim. Cosmochim. Acta* **149**, 46-63.

Hellmann J. L., Kruijer T. S., Van Orman J. A., Metzler K. and Kleine, T. (2019) Hf-W chronology of ordinary chondrites. *Geochim. Cosmochim. Acta* **258**, 290-309.

Humayun M. and Campbell, A. J. (2002). The duration of ordinary chondrite metamorphism inferred from tungsten microdistribution in metal. *Earth Planet. Sc. Lett.* **198(1-2)**, 225-243.

Hutchison R., Alexander C. M. O. and barber D. J. (1987) The Semarkona meteorite: First recorded occurrence of smectite in an ordinary chondrite, and its implications. *Geochim. Cosmochim. Acta* **51**, 1875–1882.

Jarosewich E. (1990) Chemical analyses of meteorites: A compilation of stony and iron meteorites analyses. *Meteoritics* **25**, 323-337.

Kallemeyn G. W., Rubin A. E., Wang D. and Wasson J. T. (1989) Ordinary chondrites: Bulk compositions, classification, lithophile-element fractionations and composition-petrographic type relationships. *Geochim. Cosmochim. Acta* **53**, 2747–2767.

Kegler P. and Holzheid A. (2011) Determination of the formal Ge-oxide species in silicate melts at oxygen fugacities applicable to terrestrial core formation scenarios. *ejm* **23**, 369–378.

Kita N. T., Nagahara H., Tachibana S., Tomomura S., Spicuzza M. J., Fournelle J. H. and Valley J. W. (2010) High precision SIMS oxygen three isotope study of chondrules in LL3 chondrites: Role of ambient gas during chondrule formation. *Geochim. Cosmochim. Acta* **74**, 6610–6635.

Kleine T., Touboul M., Van Orman J. A., Bourdon B., Maden C., Mezger K. and Halliday A. N. (2008) Hf–W thermochronometry: Closure temperature and constraints on the accretion and cooling history of the H chondrite parent body. *Earth Planet. Sc. Lett.* **270**, 106–118.

Krot A. N., Keil K., Scott E. R. D., Goodrich C. A. and Weisberg M. K. (2014). Classification of meteorites and their genetic relationships. *Meteorites and cosmochemical processes*, 1-63.

Krot A. N., Zolensky M. E., Wasson J. T., Scott E. R. D., Keil K. and Ohsumi K. (1997) Carbide-magnetite assemblages in type-3 ordinary chondrites. *Geochim. Cosmochim. Acta* **61**, 219–237.

Lauretta D. S., Lodders K., Fegley B. and Kremser D. T. (1997) The origin of sulfide-rimmed metal grains in ordinary chondrites. *Earth Planet. Sc. Lett.* **151**, 289–301.

Lichtenberg T., Golabek G. J., Dullemond C. P., Schönbächler M., Gerya T. V. and Meyer M. R. (2018) Impact splash chondrule formation during planetesimal recycling. *Icarus* **302**, 27–43.

Lodders K., Palme H. and Gail H. (2009) Abundances of the elements in the solar system. In LandoltBörnstein, New Series, Vol. VI/4B, Chap. 4.4, J.E. Trümper (ed.), Berlin, Heidelberg, New York: Springer-Verlag,p. 560-630.

Luais B. (2012) Germanium chemistry and MC-ICPMS isotopic measurements of Fe–Ni, Zn alloys and silicate matrices: Insights into deep Earth processes. *Chem. Geol.* **334**, 295–311.

Luais B. (2007) Isotopic fractionation of germanium in iron meteorites: Significance for nebular condensation, core formation and impact processes. *Earth Planet. Sc. Lett.* **262**, 21–36.

Luais B, Le Carlier de Veslud C., Géraud Y., Gauthier-Lafaye F. (2009) Comparative behavior of Sr, Nd and Hf isotopic systems during fluid-related deformation at middle crust levels. *Geochim. Cosmochim. Acta* **73**, 2961-2977.

Mare E. R., Tomkins A. G. and Godel B. M. (2014) Restriction of parent body heating by metal-troilite melting: Thermal models for the ordinary chondrites. *Meteorit Planet Sci* **49**, 636–651.

Mason B. (1963) Olivine composition in chondrites. *Geochim. Cosmochim. Acta* **27**, 1011–1023.

McDermott K. H., Greenwood R. C., Scott E. R. D., Franchi I. A. and Anand M. (2016) Oxygen isotope and petrological study of silicate inclusions in IIE iron meteorites and their relationship with H chondrites. *Geochim. Cosmochim. Acta* **173**, 97–113.

McSween H. Y. and Labotka T. C. (1993) Oxidation during metamorphism of the ordinary chondrites. *Geochim. Cosmochim. Acta* **57**, 1105–1114.

Monnereau M., Toplis M. J., Baratoux D. and Guignard J. (2013) Thermal history of the H-chondrite parent body: Implications for metamorphic grade and accretionary time-scales. *Geochim. Cosmochim. Acta* **119**, 302–321.

Okabayashi S., Yokoyama T., Nakanishi, N. and Iwamori, H. (2019). Fractionation of highly siderophile elements in metal grains from unequilibrated ordinary chondrites: Implications for the origin of chondritic metals. *Geochim. Cosmochim. Acta* **244**, 197-215.

Olsen E. and Jarosewich E. (1971) Chondrules: First Occurrence in an Iron Meteorite. *Science* **174**, 583–585.

Reisener R. J. and Goldstein J. I. (2003) Ordinary chondrite metallography: Part 1. Fe-Ni taenite cooling experiments. *Meteorit. Planet. Sci.* **38**, 1669–1678.

Reisener R. J., Goldstein J. I. and Petaev M. I. (2006) Olivine zoning and retrograde olivine-orthopyroxene-metal equilibration in H5 and H6 chondrites. *Meteorit. Planet. Sci.* **41**, 1839–1852.

Richter F.M. (2004) Timescales determining the degree of kinetic isotope fractionation by evaporation and condensation. *Geochim. Cosmochim. Acta* **23**, 4971-4992.

Romig A. D. and Goldstein J. I. (1978) Determination of the Fe-rich portion of the Fe-Ni-C phase diagram. *MTA* **9**, 1599–1609.

Rouxel O. J. and Luais B. (2017) Germanium Isotope Geochemistry. *Rev. Mineral. Geochem.* **82**, 601–656.

Rubin A. E. (1990) Kamacite and olivine in ordinary chondrites: Intergroup and intragroup relationships. *Geochim. Cosmochim. Acta* **54**, 1217–1232.

Rubin A. E. (1994) Metallic copper in ordinary chondrites. *Meteoritics* **29**, 93–98.

Rubin A. E. (2003) Chromite-plagioclase assemblages as a new shock indicator; implications for the shock and thermal histories of ordinary chondrites. *Geochim. Cosmochim. Acta* **67**, 2695–2709.

Rubin A. E. (2005) Relationships among intrinsic properties of ordinary chondrites: Oxidation state, bulk chemistry, oxygen-isotopic composition, petrologic type, and chondrule size. *Geochim. Cosmochim. Acta* **69**, 4907–4918.

Rushmer T., Petford N., Humayun M. and Campbell A. J. (2005) Fe-liquid segregation in deforming planetesimals: Coupling Core-Forming compositions with transport phenomena. *Earth Planet. Sc. Lett.* **239**, 185–202.

Ruzicka A. (2014) Silicate-bearing iron meteorites and their implications for the evolution of asteroidal parent bodies. *Chem. Erde-Geochm.* **74**, 3-48.

Ruzicka A., Killgore M., Mittlefehldt D. W. and Fries M. D. (2005) Portales Valley: Petrology of a metallic-melt meteorite breccia. *Meteorit. Planet. Sci.* **40**, 261–295.

Sears D. W. (1978) Condensation and the composition of iron meteorites. *Earth Planet. Sc. Lett.* **41**, 128–138.

Stöffler D., Keil K. and Edward R.D S. (1991) Shock metamorphism of ordinary chondrites. *Geochim. Cosmochim. Acta* **55**, 3845–3867.

Tait A. W., Tomkins A. G., Godel B. M., Wilson S. A. and Hasalova P. (2014) Investigation of the H7 ordinary chondrite, Watson 012: Implications for recognition and classification of Type 7 meteorites. *Geochim. Cosmochim. Acta* **134**, 175–196.

Tandon S. N. and Wasson J. T. (1968) Gallium, germanium, indium and iridium variations in a suite of L-group chondrites. *Geochim. Cosmochim. Acta* **32**, 1087–1109.

Tomkins A. G., Weinberg R. F., Schaefer B. F. and Langendam A. (2013) Disequilibrium melting and melt migration driven by impacts: Implications for rapid planetesimal core formation. *Geochim. Cosmochim. Acta* **100**, 41–59.

Trieloff M., Jessberger E. K., Herrwerth I., Hopp J., Fiéni C., Ghélis M., Bourot-Denise M. and Pellas P. (2003) Structure and thermal history of the H-chondrite parent asteroid revealed by thermochronometry. *Nature* **422**, 502–506.

Urey H. C. and Craig H. (1953) The composition of the stone meteorites and the origin of the meteorites. *Geochim. Cosmochim. Acta* **4**, 36–82.

Van Schmus W. R. and Wood J. A. (1967) A chemical-petrologic classification for the chondritic meteorites. *Geochim. Cosmochim. Acta* **31**, 747–765.

Wai C. M. and Wasson J. T. (1979) Nebular condensation of Ga, Ge and Sb and the chemical classification of iron meteorites. *Nature* **282**, 790.

Wai C. M. and Wasson J. T. (1977) Nebular condensation of moderately volatile elements and their abundances in ordinary chondrites. *Earth Planet. Sc. Lett.* **36**, 1–13.

Warren P. H. and Huber H. (2006) Ureilite petrogenesis: A limited role for smelting during anatexis and catastrophic disruption. *Meteorit. Planet. Sci.* **41**, 835–849.

Wasson J. T. (2017) Formation of non-magmatic iron-meteorite group IIE. *Geochim. Cosmochim. Acta* **197**, 396–416.

Wasson J. T. (1972) Formation of ordinary chondrites. *Rev. Geophys.* **10(3)**, 711-759.

Wasson J. T. (1974) *Meteorites: Classification and Properties*., Springer-Verlag, Berlin Heidelberg.

Wasson J. T. (2000) Oxygen-isotopic evolution of the solar nebula. *Rev. Geophys.* **38**, 491–512.

Wasson J. T. and Kallemeyn G. W. (1988) Compositions of Chondrites. In *Philosophical Transactions of the Royal Society A: Mathematical, Physical and Engineering Sciences* **325**, 535–544.

Wasson J. T. and Krot A. N. (1994) Fayalite-silica association in unequilibrated ordinary chondrites: Evidence for aqueous alteration on a parent body. *Earth Planet. Sc. Lett.* **122**, 403–416.

Wasson J.T. and Wang J. (1986) A nonmagmatic origin of group-IIE iron meteorites. *Geochim. Cosmochim. Acta* **50**, 725-732.

Wood B. J., Smythe D. J. and Harrison T. (2019). The condensation temperatures of the elements: A reappraisal. *Am. Mineral.* ***104*****(6)**, 844-856.

Yoneda S. and Grossman L. (1995) Condensation of CaOMgOAl2O3SiO2 liquids from cosmic gases. *Geochim. Cosmochim. Acta* **59**, 3413–3444.

Zanda B. (2004) Chondrules. *Earth Planet. Sc. Lett.* **224**, 1–17.

Zanda B., Hewins R., Bourot-Denise M., Bland P. and Albarede F. (2006) Formation of solar nebula reservoirs by mixing chondritic components. *Earth Planet. Sc. Lett.* **248**, 650–660.

Figure Captions

Figure 1: (A) Elemental compositions of the bulk meteorites (filled circles), metal (diamond), silicate (empty circle), and sulfide (square) from H (in blue), L (in red), and LL (in green) ordinary chondrites. Data shows large variation among all phases. The germanium concentration decreases from the metal (60 to 170 ppm as a function of the chondrite group) to bulk (≈10 to 20 ppm) to silicate (≈0.1 to 1 ppm) to sulfide (≈2 ppb) phases. There is no variation associated with the petrologic type. (B) A detailed view, in log scale, of the low Ge silicates and sulfide phases (dashed rectangle of A). Table 1 lists all abbreviations.

Figure 2: (A) A detailed view of the $\delta^{74/70}$Ge isotopic compositions among the bulk, metal, and silicate in the H ordinary chondrites. The meteorites are ordered from the least metamorphosed (Dhajala H3.4) to highest (Guareña H6) types. Rose City and Portales Valley are plotted separately due to their specific textures (see text). The $\delta^{74/70}$Ge compositions become lighter from metal, to bulk sample, and, finally, to silicate. Silicates display larger $\delta^{74/70}$Ge variations than the metal and bulk samples. Isotopic fractionation between the phases are: $\Delta^{74/70}Ge_{bulk\text{-}metal}$= –0.03 ± 0.21‰, $\Delta^{74/70}Ge_{bulk\text{-}silicate}$ = 0.16 ± 0.33‰, $\Delta^{74/70}Ge_{bulk\text{-}sulfide}$ = 1.06 ± 0.16‰, and $\Delta_{metal\text{-}silicate}{}^{74/70}$Ge = 0.22 ± 0.36‰. (B) A comparison of the $\delta^{74/70}$Ge metal values between the H (blue diamonds), L (red diamonds), and LL (green diamond) groups. All meteorites from the H and L and LL groups are plotted, with mean values of H_{mean}= –0.51 ± 0.09‰, L_{mean} = –0.31 ± 0.06‰, and LL_{mean} = –0.26 ± 0.09‰. The value for Dhajala was not included in the mean value for H due to its off-trend isotopic composition (see section 4.5 for more details). Identical abbreviations as Fig. 1 and Table 1.

Figure 3: (A) $\delta^{74/70}$Ge versus log(Ge) concentration of the bulk and mineral phases of the H, L, and LL ordinary chondrites. (B) Negative correlation between $\delta^{74/70}$Ge and log(1/[Ge]) for the metal, silicate, bulk sample, and sulfide phases in the H chondrites (R^2 = 0.85).

Figure 4: Variations in the germanium isotopic composition and isotopic fractionation for H ordinary chondrites. (A) Correlation between $\Delta^{74/70}Ge_{metal\text{-}silicate}$ and $\Delta^{74/70}Ge_{Bulk\text{-}silicate}$ with a slope of 1.2 (R^2 = 0.9). Metal and bulk Ge isotopic compositions are similar within a 2σ SD. (B) $\Delta^{74/70}Ge_{metal\text{-}silicate}$ versus $\delta^{74/70}Ge_{metal}$ shows no isotopic variation for metals among the petrologic groups. Values are from Table 4.

Figure 5: (A) The Ge elemental composition versus %Fa in olivine for the three OC groups. All data plot near the regression line (R^2 = 0.92). (B) $\delta^{74/70}$Ge of the metal phase versus %Fa in olivine for the H, L, and LL groups. Both the H and L groups plot near the regression line, where no clear correlation occurs within the groups. There

is no data for %Fa for Parnalle due to its large range in olivine composition (e.g., Rubin, 1990). Ge data for LL for Sako-Banja (SB), Cherokee Spring (CS), Olivenza, (Olz), Paragould (Prg), Dhurmsala (Drm), and Mangwendi (Mgw) are from Chou and Cohen (1973) and %Fa data are from Dodd (1968) and Dunn et al. (2010). See Table 5 for other references and %Fa.

Figure 6: $\delta^{74/70}$Ge of the metal phase versus Δ^{17}O of the bulk sample for type 3 to 6 ordinary chondrites. Δ^{17}O values are from Clayton et al. (1991). Rectangles in color represent fields of Δ^{17}O variations (1σ SD) calculated from data reported in Clayton et al. (1991) and $\delta^{74/70}$Ge variations (2σ SD). Note that Dhajala value was not included in the H mean because due to its special isotopic composition (see section 4.5 for more details). The dotted line is a linear regression calculated for all individual values (R^2 = 0.676). %Fa, Δ^{17}O data, and references are given in Table 5.

Figure 7: (A) Germanium isotopic compositions versus oxygen isotopic compositions for the two chondrule fractions from Dhajala (< 300 µm are filled blue diamonds and > 300 µm are empty blue diamond). The x-axis oxygen isotopic compositions for the < 300 µm and > 300 µm size fraction chondrules are the variations reported in Clayton et al. (1991). Blue, red, and green circles represent averages of the germanium and oxygen isotopic compositions for the H, L, and LL groups, respectively. Oxygen isotopic compositions and references are given in Table 5. (B) Theoretical Type I and II chondrules and matrix germanium isotopic composition based on chondrules and matrix mixing calculations. All data for the chondrules, matrix proportions (type I = 45%, 28 % and 22%; type II = 36%, 58%, and 61%; matrix = 12.4%, 10.2%, and 15.4%, for H, L, and LL, respectively), and their respective oxygen isotopic compositions are from Zanda et al. (2006). The calculated Ge isotopic compositions of $\delta^{74/70}Ge_{type\ I}$ = –0.81‰, $\delta^{74/70}Ge_{type\ II}$ = +2.15‰, and $\delta^{74/70}Ge_{matrix}$ = –7.35‰ do not agree with the measurements of $\delta^{74/70}$Ge in chondrules displayed in Figure 7A.

Figure 8: Modelling of the Germanium content (ppm) in phyllosilicate required to change the germanium isotopic composition from an H (–0.51‰) to LL chondrite composition (–0.26‰) as a function of the accreted amount of phyllosilicates and their $\delta^{74/70}Ge_{phyllosilicate}$ composition at 1‰, 2‰, 3‰, 4‰, 5‰, 10‰, 15‰, and 20‰. The blue dashed line corresponds to $\delta^{74/70}Ge_{phyllosilicate}$ = +2.5‰, representing the isocurve that matches the Δ^{17}O of ≈+7‰ reported in Choi et al. (1998) (see text). The horizontal dark blue line is the mean Ge content in terrestrial phyllosilicates (3.8 ppm; Bernstein, 1985, and references therein) and the dark blue zone is the 2σ SD of the mean. The highlighted area in black represents the likely composition of the phyllosilicates (see the text for more

details). The forbidden zone can be defined beyond the maximum percentage of matrix in ordinary chondrites (15%; Krot et al., 2014) and maximum Ge content in terrestrial phyllosilicatse (up to 8.5 ppm; Bernstein, 1985).

Figure 9: $\Delta^{17}O$ of silicates (bulk ordinary chondrites and silicate inclusions of IIE iron meteorites) versus $\delta^{74/70}Ge$ of the metal phase in ordinary chondrites and IIE iron meteorites. The positive correlation between the IIE iron meteorites and LL ordinary chondrites demonstrates that the IIE parent body could have formed on a distinct and more reduced parent body than the H ordinary chondrite body, known as the HH parent body. As the $\Delta^{17}O$ of the NWA-118 sample is low compared to other LL chondrites, we also report the mean $\delta^{74/70}Ge$ versus $\Delta^{17}O$ for the LL chondrites (green square). References for the oxygen isotopic compositions are given in Table 5. The Ge isotopic composition of the IIE iron meteorites are from Luais (2007, 2012).

Appendix

Figure A: Germanium, nickel, and cobalt concentrations of the bulk and metal from H ordinary chondrites. (1) Co versus Ni: the Allegan (H5) metal phase exhibits high Ni and low Co contents that are characteristic of a taenite phase compared with kamacite. (2) Ge versus Ni: the high Ge contents of Allegan suggest a nugget effect that characterizes the Ni-rich, Co-poor taenite phase. Same legend for (1) and (2).

Figure B: $\delta^{74/70}$Ge versus $\delta^{72/70}$Ge of bulk, silicates, metal, and sulfide from the H group, and the metal phase from the L and LL groups of the ordinary chondrites. Error bars are 2σ SD. Except for sulfides, all standards and samples fall within error of the mass-dependent fractionation line, which is also the terrestrial mass fractionation line (TMFL) (Luais, 2007). Large errors for sulfide result from the small amount of measured Ge due to its low Ge concentration. Ge isotopic compositions become lighter from metal to bulk, silicate, and, then, to the sulfide phase. Identical trends as the $\delta^{74/70}$Ge versus $\delta^{73/70}$Ge diagram.

Figure1

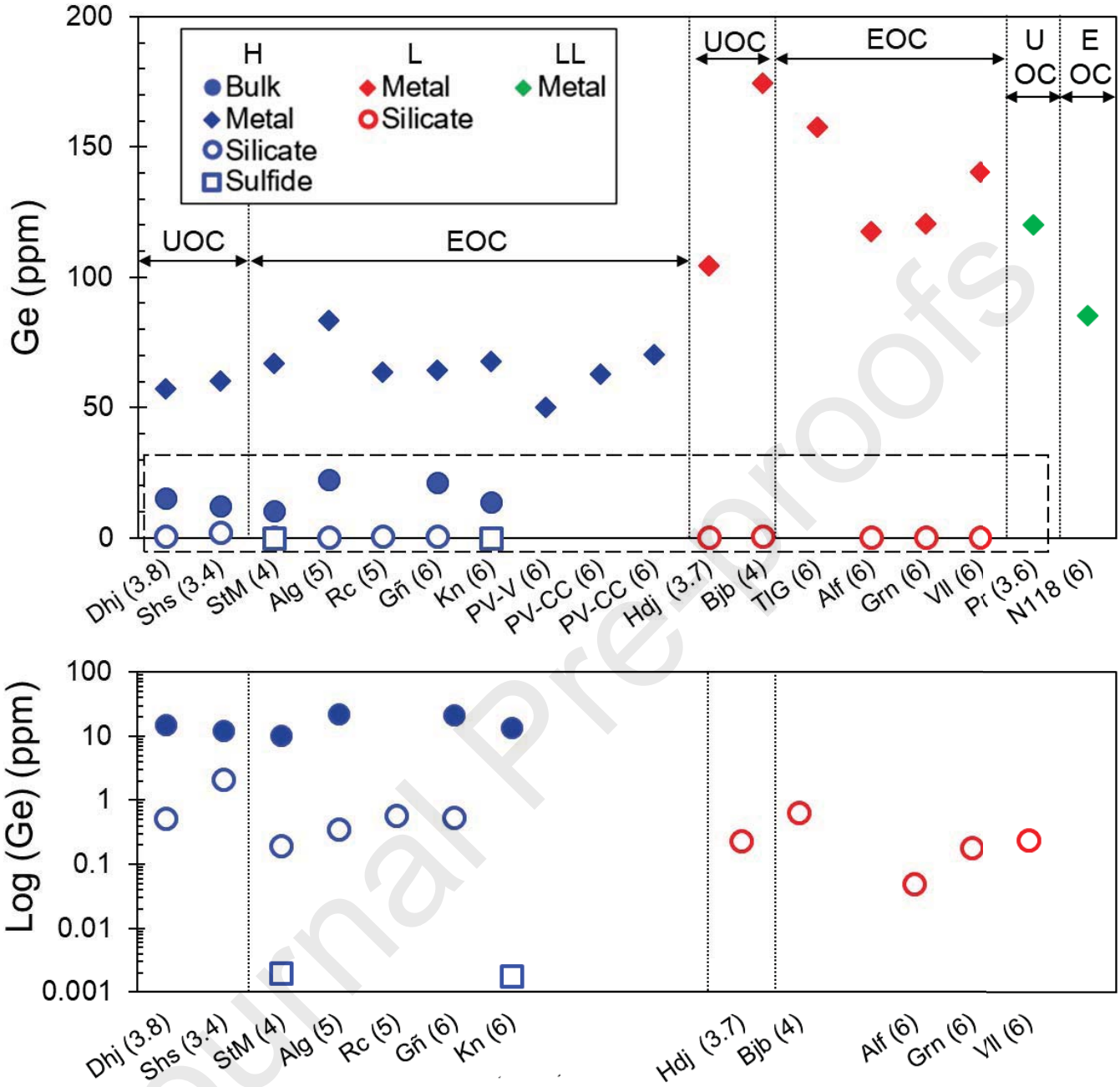

Figure 1, Florin et al., 2019

Figure2

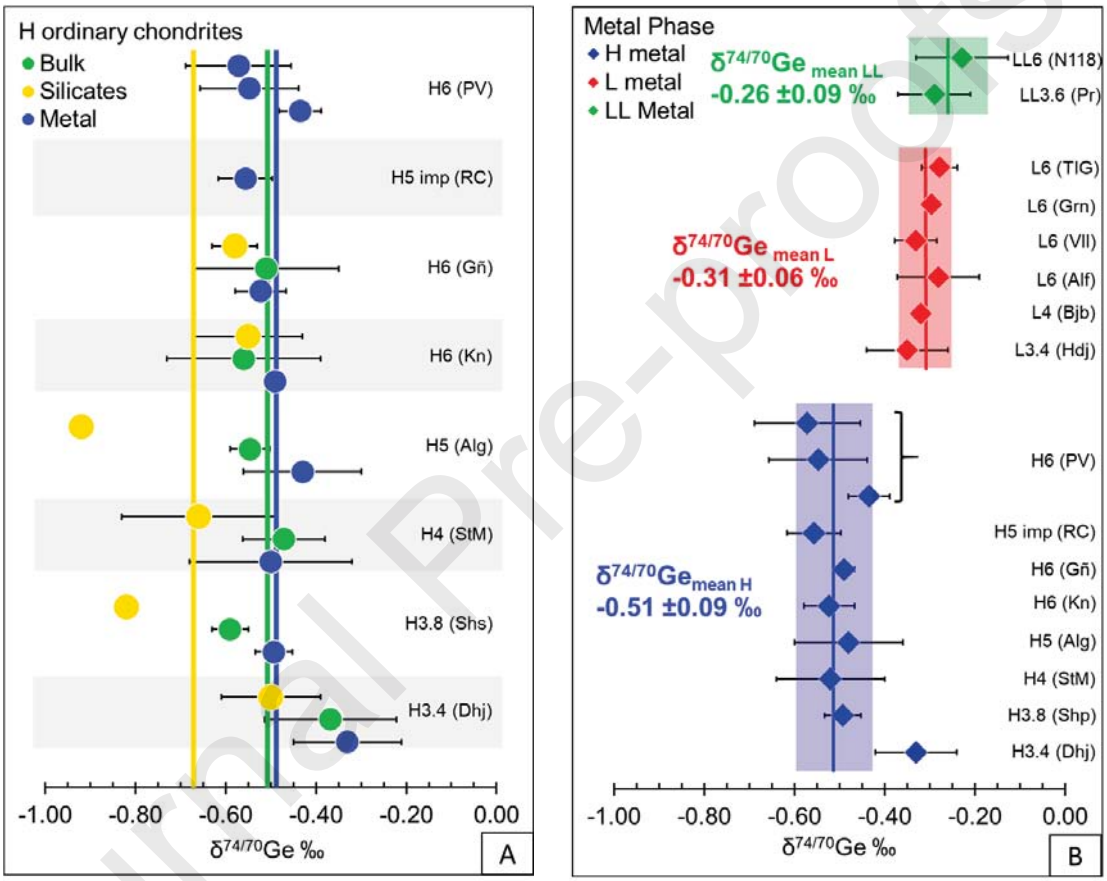

Figure 2, Florin et al., 2019

Figure3

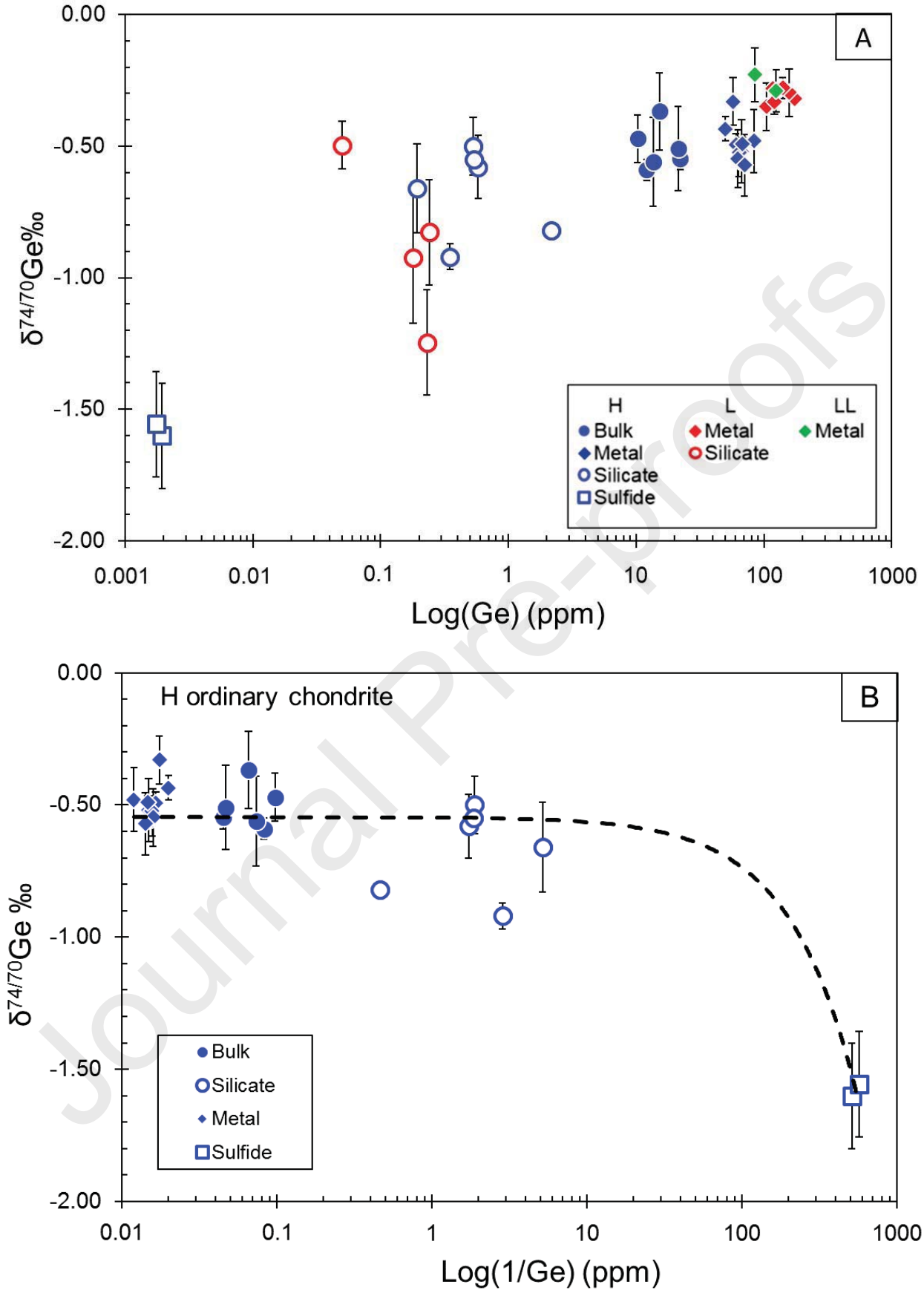

Figure 3, Florin et al., 2019

Figure 4

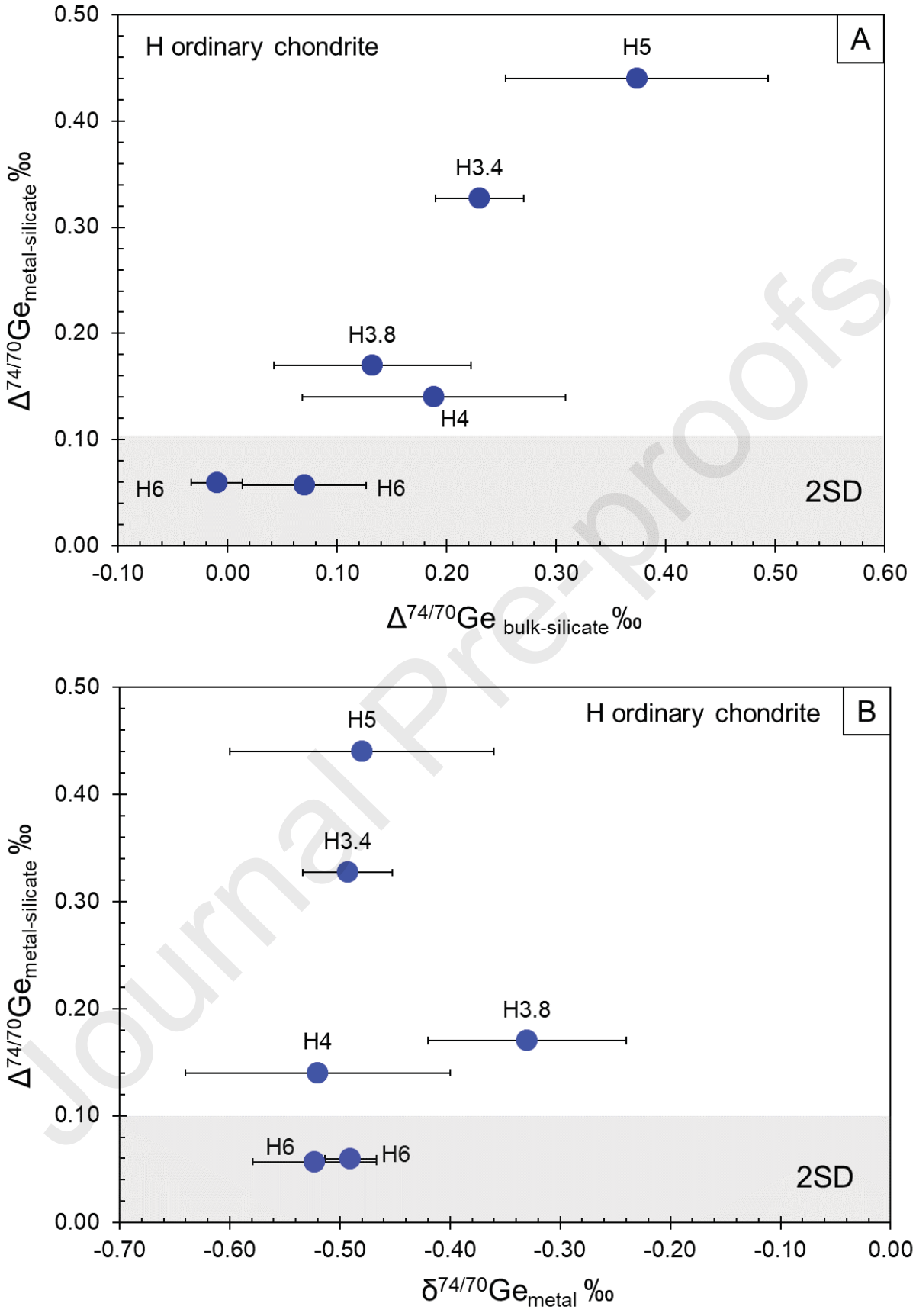

Figure 4, Florin et al., 2019

Figure5

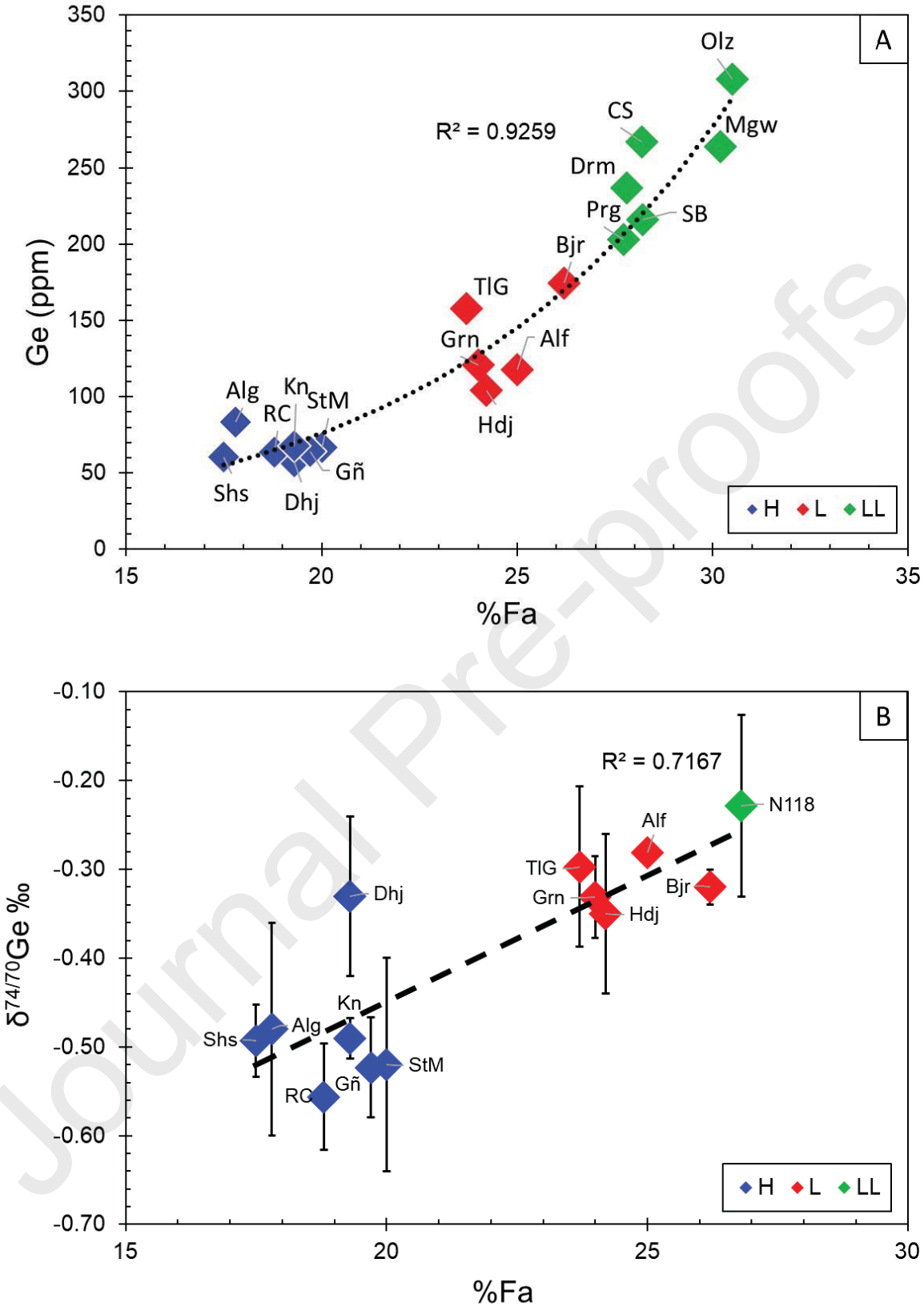

Figure 5, Florin et al., 2019

Figure 6

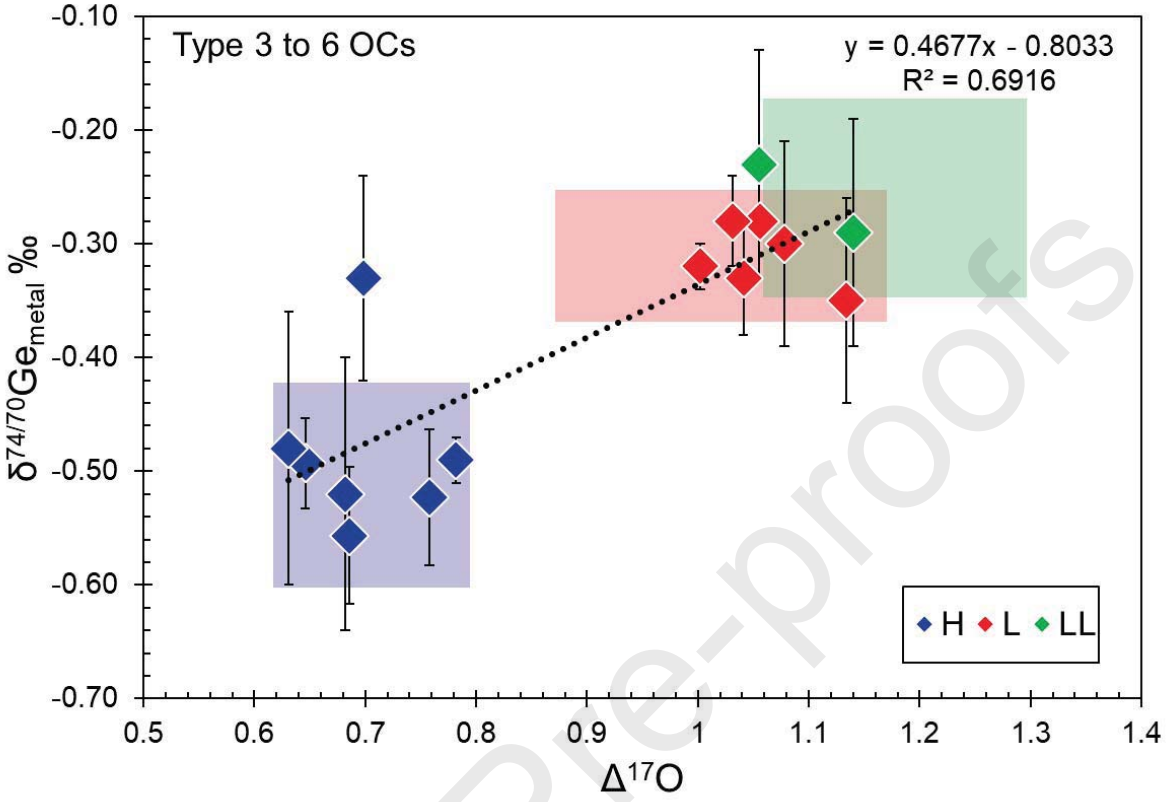

Figure 6, Florin et al., 2019

Figure7

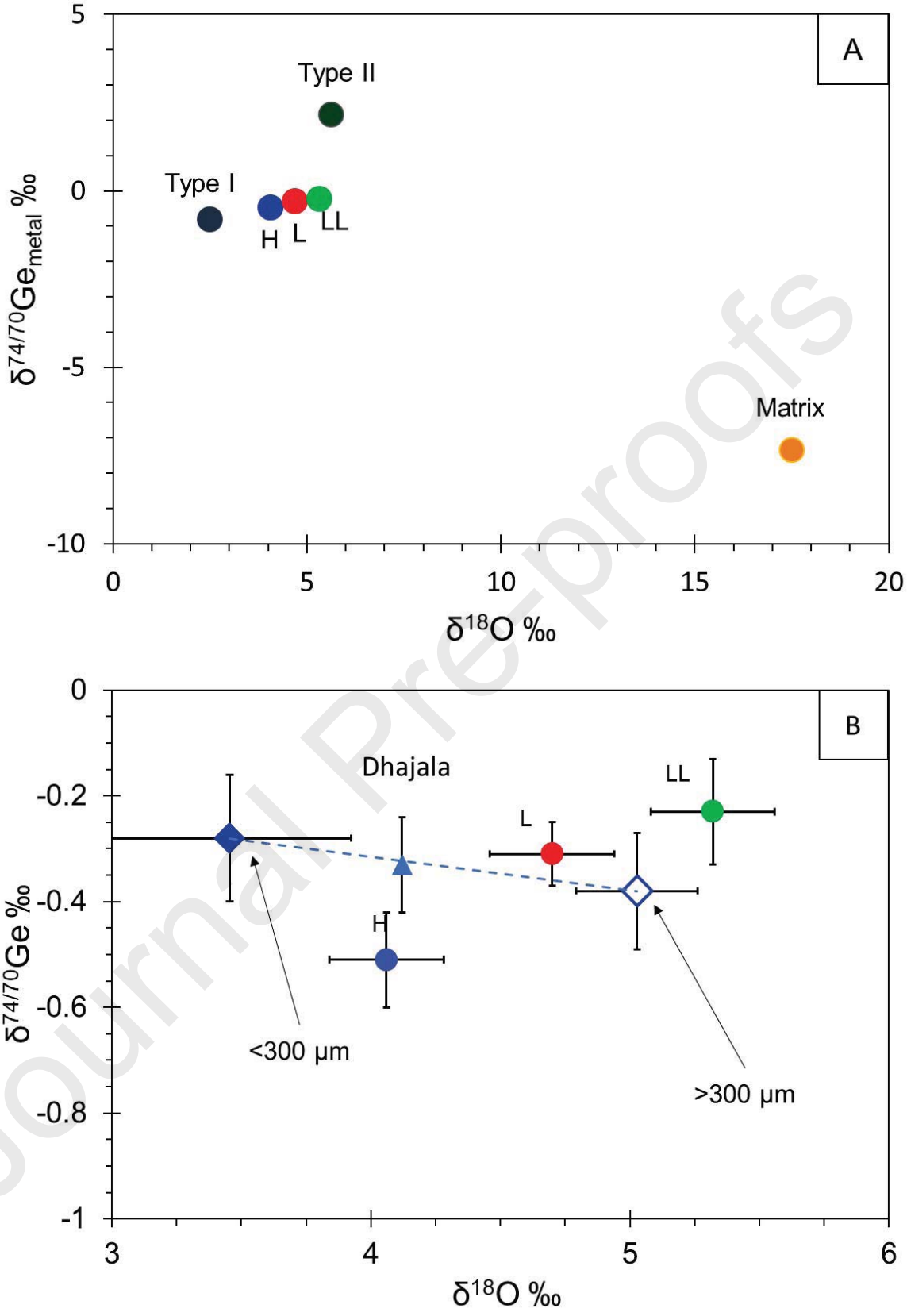

Figure 7, Florin et al., 2019

Figure8

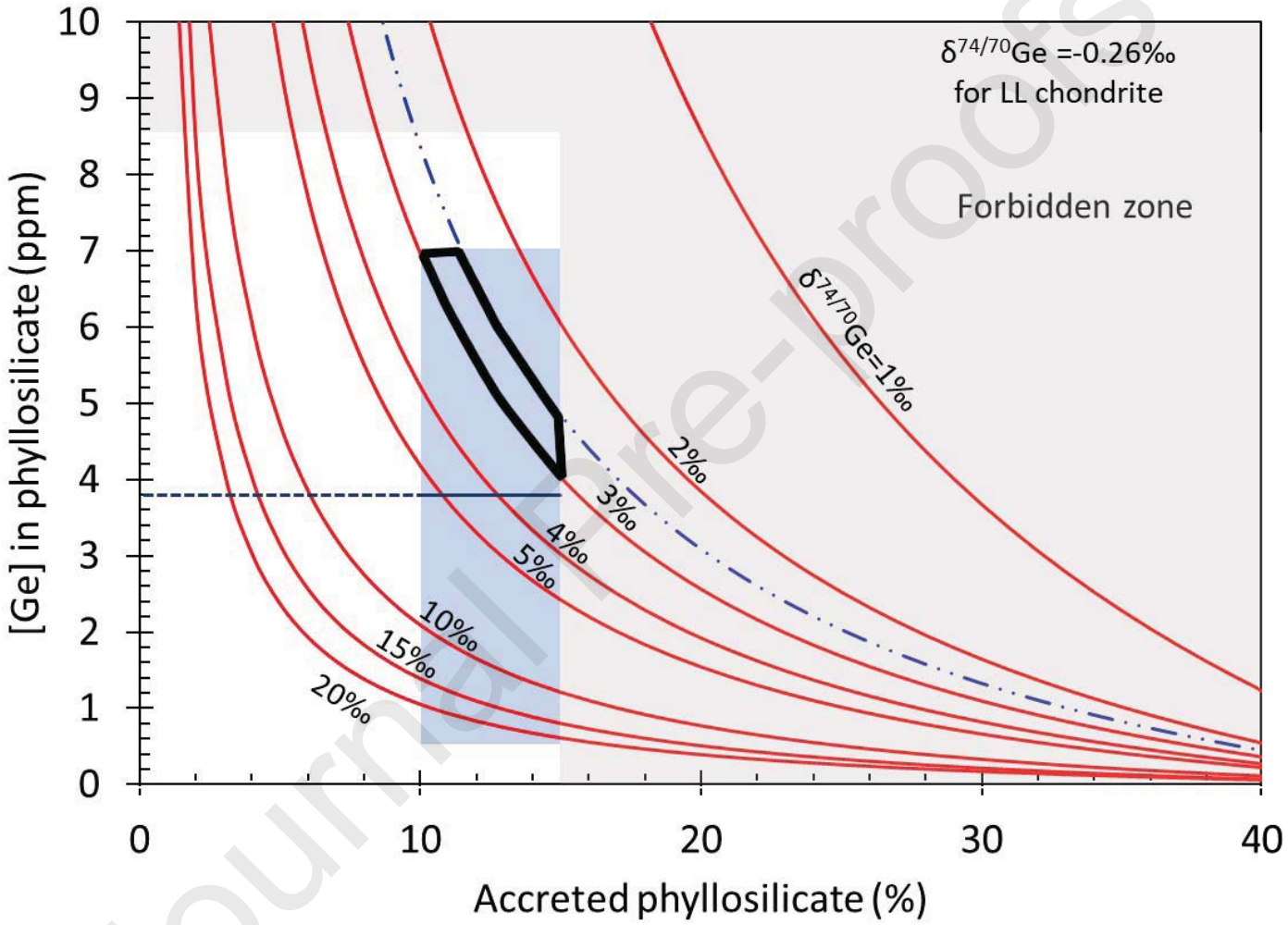

Figure 8, Florin et al., 2019

Figure9

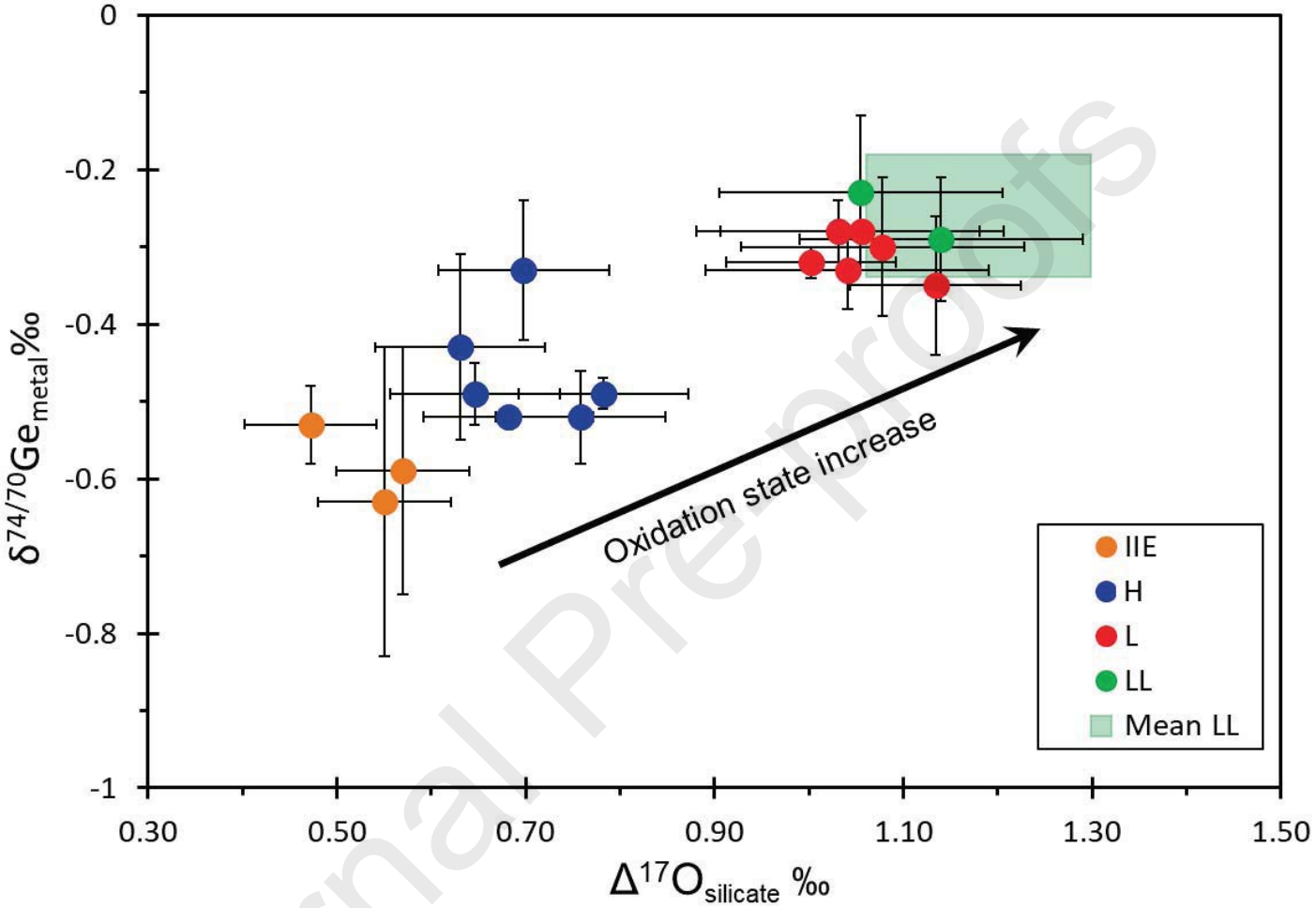

Figure 9, Florin et al., 2019

Table 1. The H, L, and LL ordinary chondrites analyzed in this study, with their petrologic types and shock stages. All meteorites are falls.

Samples	Sample N° (Sources)	Petrologic types	Shock stage and references
Sharps (Shs)	USNM 640 (SI)	H3.4	S3 (1)
Dhajala (Dhj)	USNM 5832 (SI)	H3.8	S1 (1)
St Marguerite (StM)	MNHN 3290 (MNHN-Paris)	H4	S2 (2)
Allegan (Alg)	USNM 215 (SI)	H5	S1 (2)
Rose city (RC)	USNM 6771 (SI)	H5 IB	S6 (1)
Guarena (Gn)	(MNCN)	H6	S1 (3)
Kernouvé (Kn)	(Smithsonian)	H6	S1 (3)
Portales Valley (PV)	USNM 6975 (SI)	H6	S1 (3)
Herdjaz (Hdj)	MNHN 2132 (MNHN-Paris)	L3.7	S4 (2)
Björbole (Bjb)	USNM 6705 (SI)	L4	S1 (5)
Tourine la Grosse (TlG)	MNHN 191 (MNHN-Paris)	L6	S3 (5)
Alfianello (Alf)	MNHN 885 (MNHN-Paris)	L6	S5 (2)
Vouillé (Vll)	MNHN 148 (MNHN-Paris)	L6	S5 (4)
Granes (Grn)	MNHN 2852 (MNHN-Paris)	L6	NA
Parnalle (Pr)	USNM 1613 (SI)	LL3.6	
NWA 118 (N118)	Private collection	LL6	S3 (7)

[1]: Stöffler (1991); [2]: Rubin (1994); [3]: Reisener And Goldstein (2003); [4]: Rubin (2003); [5]: Dodd and Jarosewich (1979); [6]: Bennett and Mc Sween (1996); [7]: Grossman and Zipfel (2001).

Abbreviations: MNCN, Museo Nacional de Ciencias Naturales, Madrid; MNHN, Muséum National d'Histoire Naturelle, Paris; SI, Smithsonian; USNM, United States National Museum, Washington; IB, Impact Breccia

Table 2. The Ge isotopic compositions of standards and geostandards, cleaning tests on San Carlos olivines for silicate purification, and BIR-1 digestion in Bola Teflon bombs at 150°C and 25 bar. Germanium concentrations were measured using an ICP-MS *X-Series* at CRPG, with a precision of less than 2%. n is the number of replicates.

	Ge ppm	$\delta^{72/70}$Ge ‰	± 2SD	$\delta^{73/70}$Ge ‰	± 2SD	$\delta^{74/70}$Ge ‰	± 2SD	n
In-house standard								
Magura (IAB iron)	427[(1)]	0.42	0.06	0.58	0.11	0.78	0.08	19
Standard solutions								
JMC-Ge		–0.15	0.08	–0.19	0.13	–0.32	0.11	95
Aldrich-Ge		–1.01	0.07	–1.52	0.13	–1.97	0.12	99
Geostandards								
BIR-1								
Hotplate digestion	1.52[(2)]	0.32	0.04	0.42	0.07	0.59	0.06	7
Bomb digestion	1.50	0.31	0.05	0.42	0.14	0.59	0.01	3
San Carlos Olivines								
Un-cleaned	0.89	0.35	0.04	0.48	0.08	0.70	0.08	3
Cleaned	0.90	0.36	0.03	0.47	0.14	0.71	0.09	3

[(1)]Value from Luais (2007). [(2)]Value from Luais (2012).

Samples	Ni (wt%)	Co (ppm)	Co/Ni	Ge (ppm)	$\delta^{72/70}$Ge ‰	± 2SD	$\delta^{73/70}$Ge ‰	± 2SD	$\delta^{74/70}$Ge ‰	± 2SD	N
H ordinary chondrites											
Bulk											
Dhajala (H3.8)	1.22	850	0.070	15.2	–0.16	0.06	–0.25	0.12	–0.37	0.15	8
Sharps (H3.4)	1.26	668	0.053	12.1	–0.29	0.06	–0.49	0.15	–0.59	0.04	3
Ste. Marguerite (H4)	0.83	580	0.070	10.3	–0.23	0.06	–0.37	0.11	–0.47	0.09	4
Allegan (H5)	1.52	1448	0.095	22.2	–0.2	0.07	–0.33	0.1	–0.55	0.04	3
Guareña (H6)	1.59	1123	0.071	21.4	–0.23	0.09	–0.38	0.13	–0.51	0.16	11
Kernouvé (H6)	1.27	776	0.061	13.6	–0.29	0.12	–0.45	0.17	–0.56	0.17	10
Mean	*1.28*	*908*	*0.070*	*15.8*	*–0.23*	*0.1*	*–0.38*	*0.17*	*–0.54*[(1)]	*0.09*	
Metal											
Dhajala (H3.8)	6.79	4746	0.070	57.3	–0.16	0.1	–0.23	0.13	–0.33	0.09	8
Sharps (H3.4)	7.78	4543	0.058	60.3	–0.24	0.02	–0.38	0.04	–0.49	0.04	5
Ste. Marguerite (H4)	9.07	4940	0.054	67.0	–0.23	0.13	–0.36	0.21	–0.52	0.12	8
Allegan (H5)	22.11	2527	0.011	83.5	–0.25	0.11	–0.38	0.17	–0.48	0.12	8
Roses City Veins (H5)	7.14	4200	0.059	63.1	–0.25	0.03	–0.36	0.05	–0.56	0.06	3
Guareña (H6)	9.44	4893	0.052	64.2	–0.19	0.24	–0.31	0.37	–0.52	0.06	4
Kernouvé (H6)	9.24	5280	0.057	67.8	–0.24	0.03	–0.37	0.05	–0.49	0.02	3
Portales Valley V (H6)	9.65	4724	0.049	50.0	–0.19	0.05	–0.34	0.08	–0.43	0.05	3
Portales Valley CC(H6)	7.3	5038	0.069	62.8	–0.26	0.07	–0.4	0.01	–0.55	0.11	3
Portales Valley C (H6)	8.83	4587	0.052	70.5	–0.28	0.03	–0.4	0.05	–0.57	0.12	3
Mean	*9.74*	*4548*	*0.053*	*64.6*	*–0.23*	*0.07*	*–0.35*	*0.1*	*–0.51*[(1)]	*0.09*	
Silicate											
Dhajala (H3.8)				0.5	–0.26	0.03	–0.39	0.14	–0.50	0.11	3
Sharps (H3.4)				2.2	–0.42	0	–0.63	0.01	–0.82	0.01	3
Ste. Marguerite (H4)				0.2	–0.32	0.1	–0.53	0.07	–0.66	0.17	3
Allegan (H5)				0.4	–0.41		–0.67		–0.92		1
Guareña (H6)				0.6	–0.31	0.04	–0.47	0.1	–0.58	0.05	3
Kernouvé (H6)				0.5	–0.27	0.06	–0.42	0.11	–0.55	0.12	3
Mean				*0.7*	*–0.33*	*0.14*	*–0.52*	*0.23*	*–0.67*	*0.33*	
Sulfide [(2)]											
Ste. Marguerite (H4)				0.002					–1.60	-	1
Kernouvé (H6)				0.002	–0.59	-			–1.56	-	1
Mean				*0.002*					*–1.58*	*0.02*	
Chondrules: Dhajala											
<300µm fraction					–0.17	0.06	–0.27	0.05	–0.28	0.12	2
>300µm fraction					–0.21	0.06	–0.32	0.03	–0.38	0.11	3
L ordinary chondrites											
Metal											
Hedjaz (L3.7)	10.06	5766	0.057	104.3	–0.16	0.12	–0.3	0.11	–0.35	0.09	3

Björbole (L4)	18.15	8400	0.046	174.5	–0.16	0.03	–0.24	0.04	–0.32	0.02	3
Alfianello (L6)	11.6	7042	0.061	117.5	–0.11	0.03	–0.19	0.03	–0.28	0.01	2
Granes (L6)	15.76	5242	0.033	120.7	–0.16	0.01	–0.25	0.03	–0.33	0.05	3
Tourine la Grosse (L6)	21.21	5466	0.026	157.8	–0.17	0.07	–0.24	0.07	–0.3	0.09	4
Vouillé (L6)	14.18	6806	0.048	140.4	–0.11	0.02	–0.20	0.07	–0.28	0.04	3
Mean	*15.2*	*6454*	*0.045*	*135.9*	*–0.15*	*0.05*	*–0.24*	*0.08*	*–0.31*	*0.06*	
Silicate											
Hedjaz (L3.7)				0.23	–0.32	0.02	–0.58	0.41	–0.85	0.22	2
Björbole (L4)				0.65	–0.27	0.05	–0.40	0.12	–0.50	0.09	5
Alfianello (L6)				0.05	–0.57		–0.92		–1.25		1
Granes (L6)				0.18	–0.44	0.21	–0.69	0.07	–0.92	0.25	2
Vouillé (L6)				0.24	–0.22		–0.51		–0.83		1
Mean				*0.27*	*–0.36*	*0.09*	*–0.62*	*0.2*	*–0.87*	*0.18*	
LL ordinary chondrites											
Metal											
Parnalle (LL3.6)				120	–0.18	0.07	–0.31	0.17	–0.29	0.08	3
NWA 118 (LL6)				85	–0.13	0.06	–0.19	0.1	–0.23	0.10	4
Mean				*102.5*	*–0.16*	*0.07*	*–0.25*	*0.2*	*–0.26*	*0.09*	

Table 3. The Ni, Co, and Ge concentrations, as well as the $\delta^{72/70}$Ge, $\delta^{73/70}$Ge, and $\delta^{74/70}$Ge values of the ordinary chondrites relative to NIST 3120a. Reproducibility is given as 2SD. N is the number of replicates for $\delta^{72/70}$Ge, $\delta^{73/70}$Ge, and $\delta^{74/70}$Ge. Error of less than 5% for the Ge, Ni, and Co elemental compositions.

(1) Dhajala was excluded from the mean due to its unusual Ge isotopic composition, see section 4.3 for explanations.[(2)] There is no standard deviation for sulfide because only one measurement was done per sample due to their low concentration.

Table 4. The germanium isotopic factor among the bulk, metal, silicate, and sulfide of H ordinary chondrites, as well as the Ge elemental fractionation between metal and silicate.

Samples	$\Delta^{74/70}Ge_{bulk\text{-}metal}$	$\Delta^{74/70}Ge_{bulk\text{-}silicate}$	$\Delta^{74/70}Ge_{metal\text{-}silicate}$	$\Delta^{74/70}Ge_{bulk\text{-}sulfide}$	$DGe_{metal\text{-}silicate}$
Sharps (H3.4)	–0.10	0.23	0.33	-	38
Dhajala (H3.8)	–0.04	0.13	0.17	-	123
Ste. Marguerite (H4)	0.05	0.19	0.16	1.13	395
Allegan (H5)	–0.07	0.37	0.49	-	272
Guareña (H6)	0.01	0.07	0.06	-	126
Kernouvé (H6)	–0.07	–0.01	0.06	1.00	143
Mean	*–0.03 ± 0.21*	*0.16 ± 0.33*	*0.22 ± 0.36*	*1.06 ± 0.16*	*183*

Table 5. The oxygen Isotopic compositions and percentage of fayalite (%Fa) in ordinary chondrites.

Meteorites	%Fa	Ref	δ18O (‰)	δ17O (‰)	Δ17O (‰)	2SD	Ref
Ordinary chondrites							
Sharps	17.5	5	3.95	2.7	0.646		1
Dhajala	19.3	4	4.12	2.84	0.698		1
Ste Marguerite	20.0	9	3.59	2.54	0.682		3
Allegan	17.8	4	3.97	2.68	0.631		1
Rose City	18.8	4	3.68	2.6	0.686		2
Guareña	19.7	4	4.1	2.89	0.758		1
Kernouvé	19.3	7	4.15	2.94	0.782		1
Hedjaz	24.2	4	4.57	3.51	1.134		1
Bjurböle	26.2	4	4.9	3.55	1.002		1
Alfianelo	25.0	4	4.69	3.54	1.056		3
Granes	24.0	9	4.01	3.17	1.041		3
Vouillé	-		4.67	3.51	1.031		3
Tourine la Grosse	23.7	6	4.66	3.55	1.078		3
Parnalle	-	4	5.15	3.82	1.140		1
NWA 118	26.8	8	4.61	3.5	1.055		3
Mean H	*18.9*		*4.06*	*2.81*	*0.705*	*0.09*	
Mean L	*24.6*		*4.70*	*3.46*	*1.020*	*0.15*	
Mean LL	-		*5.32*	*3.95*	*1.180*	*0.12*	
IIE Iron meteorites							
Netschaëvo			3.46	2.37	0.57		10
Miles			4.75	3.04	0.57		10
Weekeroo station			4.11	2.58	0.62		10

References : 1: Clayton et al. (1991); 2: Folco et al. (2004); 3: This study; 4: Rubin (1990); 5: Dodd (1968); 6: Dodd & Jarosewich (1979); 7: Reisener et al. (2006); 8: Grossman & Zipfel (2001); 9: Mason (1963); 10: Clayton & Mayeda (1996)

Declaration of interests

☒ The authors declare that they have no known competing financial interests or personal relationships that could have appeared to influence the work reported in this paper.

☐The authors declare the following financial interests/personal relationships which may be considered as potential competing interests: